

RXTE OBSERVATIONS OF THE NEUTRON STAR LOW-MASS X-RAY BINARY GX 17+2: CORRELATED X-RAY SPECTRAL AND TIMING BEHAVIOR

JEROEN HOMAN¹, MICHAEL VAN DER KLIS¹, PETER G. JONKER¹, RUDY WIJNANDS^{2,3}, ERIK
KUULKERS^{4,5}, MARIANO MÉNDEZ⁶, & WALTER H. G. LEWIN⁷

Draft version December 2, 2024

ABSTRACT

We have analyzed \sim 600 ks of *Rossi X-ray Timing Explorer* data of the neutron star low-mass X-ray binary and Z source GX 17+2. A study was performed of the properties of the noise components and quasi-periodic oscillations (QPOs) as a function of the spectral properties, with the main goal to study the relation between the frequencies of the horizontal branch and upper kHz QPOs. It was found that when the upper kHz QPO frequency is below 1030 Hz these frequencies correlate, whereas above 1030 Hz they anti-correlate. GX 17+2 is the first source in which this is observed. We also found that the frequency difference of the high frequency QPOs was not constant and that the quality factors (Q values) of the HBO, its second harmonic, and the kHz QPOs are similar, and vary almost hand in hand by a factor of more than three. Observations of the normal branch oscillations during two type I X-ray bursts showed that their absolute amplitude decreased as the flux from the neutron star became stronger. We discuss these and other findings in terms of models that have been proposed for these phenomena. We also compare the behavior of GX 17+2 and other Z sources with that of black hole sources and consider the possibility that the mass accretion rate might not be driving force behind all spectral and variability changes.

Subject headings: accretion, accretion disks - stars: individual (GX 17+2) - X-rays: stars

1. INTRODUCTION

Based on their spectral and variability properties, six of the persistently bright neutron star low-mass X-ray binaries (LMXBs) were classified as Z sources (Hasinger & van der Klis 1989), after the Z-like tracks they trace out in X-ray color-color (CDs) and hardness intensity diagrams (HIDs). These sources are GX 17+2, Cyg X-2, GX 5-1, GX 340+0, Sco X-1, and GX 349+2. The Z-like tracks consist of three branches, which, from top to bottom, are referred to as the horizontal branch (HB), the normal branch (NB), and the flaring branch (FB). So far, GX 349+2 is only found on the NB and FB, whereas the other Z sources show all three branches. It is generally believed that the parameter that determines the position along the Z track is the mass accretion rate, increasing from the HB to the FB. In addition to spectral changes along the Z-track, some of the Z sources show long term changes in the shape and position of the Z-track in the CD and HID. These secular changes, as they are referred to, are clearly observed in Cyg X-2 (Kuulkers et al. 1996; Wijnands et al. 1997b), GX 5-1 (Kuulkers et al. 1994), and GX 340+0 (Kuulkers & van der Klis 1996) (the Cyg-like sources; the other Z sources are referred to as the Sco-like sources), and more recently also in GX 17+2 (Wijnands et al. 1997a). It has been suggested that they are related to the relatively high inclination at which these sources are seen (Kuulkers et al. 1994; Kuulkers & van der Klis 1995), or to a higher magnetic field strength of the neutron stars (Psaltis et al. 1995).

The power spectra of the Z sources show several types of quasi-periodic oscillations (QPOs) and noise components (see

van der Klis 1995a, for a review). It was found that their presence and properties are very well correlated with the position of the source along the Z track (Hasinger & van der Klis 1989), even when the Z-tracks show secular changes (e.g. Kuulkers et al. 1994). Three types of low frequency (<100 Hz) QPOs are seen in the Z sources: the horizontal branch (HBOs), normal branch (NBOs) and flaring branch QPOs (FBOs). Their names derive from the branches on which they were originally found. The HBO is found on the HB and NB with a frequency (15–60 Hz) that gradually increases along the HB towards the NB. When the sources move from the HB onto the NB the frequency increase flattens off. In GX 17+2 and Cyg X-2 it was found that when the source passes a certain point on the NB, the HBO frequency starts to decrease (Wijnands et al. 1996, 1997b). The NBO and FBO are most likely the same phenomenon. They are found on the NB and FB (near the NB/FB vertex) but not on the HB. On the NB the QPO has a frequency of \sim 5–7 Hz, which rapidly increases to \sim 20 Hz when the source moves across the NB/FB vertex (Priedhorsky et al. 1986; Dieters & van der Klis 2000). In recent years two types of high frequency (or kHz) QPO were found in the Z sources (van der Klis et al. 1996; Wijnands et al. 1997a, 1998a,b; Jonker et al. 1998; Zhang et al. 1998, see van der Klis 2000, for a review). They have frequencies between 215 Hz and 1130 Hz, which increase from the HB to the NB. The two QPOs are often observed simultaneously, with a frequency difference of \sim 300 Hz. In Sco X-1 this frequency difference was found to decrease with increasing QPO frequency (van der Klis et al. 1997b). The frequency difference in the other Z sources is both consistent with the be-

¹ Astronomical Institute 'Anton Pannekoek', University of Amsterdam, and Center for High Energy Astrophysics, Kruislaan 403, 1098 SJ Amsterdam, The Netherlands; homan@astro.uva.nl, michiel@astro.uva.nl, peterj@astro.uva.nl

² Center for Space Research, MIT, 77 Massachusetts Avenue, Cambridge, MA 02139-4307, USA; rudy@space.mit.edu

³ Chandra fellow

⁴ Space Research Organization Netherlands, Sorbonnelaan 2, 3594 CA Utrecht, The Netherlands; E.Kuulkers@sron.nl

⁵ Astronomical Institute, Utrecht University, P.O. Box 80000, 3508 TA Utrecht, The Netherlands

⁶ Facultad de Ciencias Astronómicas y Geofísicas, Universidad Nacional de La Plata, Paseo del Bosquey S/N, 1900 La Plata, Argentina; M.Mendez@sron.nl

⁷ Department of Physics and Center for Space Research, MIT, 77 Massachusetts Avenue, Cambridge, MA 02139-4307, USA; lewin@space.mit.edu

havior seen in Sco X-1 and with being constant (Wijnands et al. 1997a; Jonker et al. 1998; Psaltis et al. 1998). Three types of noise are seen in the Z sources. They are the very low frequency noise (VLFN), the low frequency noise (LFN), and the high frequency noise (HFN). The VLFN and HFN are found on all branches, whereas the LFN is only observed on the HB and NB. The VLFN, which is found at frequencies below 1 Hz, can be described by a power law. The HFN and LFN are both band limited components, with cutoff frequencies of, respectively, 10–100 Hz, and 2–10 Hz.

Many competing models have been proposed for the origin of the QPOs and noise components. It is beyond the scope of this introduction to mention these models in detail - most of them will be discussed in Section 4.

In this paper we present a study, based on data acquired with the *Rossi X-ray Timing Explorer (RXTE)*, of the correlated spectral and variability properties of the Z source GX 17+2. It is a continuation of the work by Wijnands et al. (1996, 1997a). The current paper constitutes the first report on the very large observing campaign of 1999, which more than doubled the total coverage of the source. This campaign was undertaken with the express purpose of investigating if a non-monotonic relation exists between the frequency of the kHz QPOs and the HBO in GX 17+2. Section 2 deals with the observations and analysis. The spectral results are presented in Section 3.1 and the results for each power spectral component in Sections 3.2 and 3.3. A number of qualitatively new results is found in our greatly expanded data set. In particular, we find that when the upper kHz QPO frequency is below 1030 Hz, it correlates with the HBO frequency, whereas above 1030 Hz they anti-correlate. We also find that kHz QPO frequency difference is not constant and that the Q values of the HBO and kHz QPOs are probably not explained by life time broadening. These and other results are compared to observations of other Z sources and discussed in terms of current models in Section 4.

2. OBSERVATIONS AND ANALYSIS

The data used for the analysis in this paper were all obtained with the Proportional Counter Array (PCA, Jahoda et al. (1996)) on board *RXTE* (Bradt et al. 1993). The PCA consists of five xenon filled proportional counter units (PCUs), each with an effective area of $\sim 1250 \text{ cm}^2$ (at 10 keV). Although the five PCUs are in principle identical they all have a slightly different energy response. These responses change continuously due to slow processes such as gas leakage and the aging of the electrodes. In addition, the high voltage settings of the instruments are occasionally altered (gain changes), resulting in rather more drastic changes in the detector response. These changes have been applied three times during the life time of *RXTE* thereby defining four gain epochs. Occasionally one or more PCUs are not operational. They can be switched off by an internal safety mechanism, or by the ground control crew, for reasons of detector preservation. Therefore, the number of active detectors varies between the observations.

All our *RXTE/PCA* observations of GX17+2 were done between 1997 February 2 and 2000 March 31. A log of the observations is given in Table 1. We do not include the observations done in February 1996, which were used by Wijnands et al. (1996). The reasons for this are the limited time resolution in the energy range of interest, difficulties with scaling the S_z due to an incomplete Z track, and the relatively small amount of data (~ 60 ks). Data taken during satellite slews and Earth oc-

culations were removed, as were the nine type I X-ray bursts that were observed; they are the subject of a separate article by Kuulkers (2001). The total amount of good data that remained was ~ 600 ks.

Data were collected in several modes with different time and spectral resolutions. Two of these modes, ‘Standard 1’ and ‘Standard 2’, were always operational. These modes have time resolutions of, respectively, 1/8 s and 16 s, and the numbers of energy channels in the 2–60 keV range are, respectively, 1 and 129. In addition to these two modes, other modes were active that varied between the observations. Their properties are given in Table 2.

The Standard 2 data were used to perform a spectral analysis. The data were background subtracted, but no dead time corrections were applied; these were in the order of 2–5%. Although dead time is intrinsically independent of energy, by not correcting for it the spectral properties are affected. The reason for this is that the model background is relatively too high compared to the total (not dead time corrected) count rate. The effects for this are strongest at high energies, where the source contribution is lowest and the background is strongest. As a result the spectrum becomes a bit softer; however, the changes in the soft and hard color are in the order of only 0.001% and 0.1%, respectively, much less than the errors due to counting statistics. In any case, we are usually not interested in the absolute values of the colors, but merely in using them as a tool to study the variability.

For each 16 s data segment (i.e. the intrinsic resolution of the Standard 2 mode) we defined two colors, which are the ratios of count rates in two different energy bands, and an intensity, which is simply the count rate in one energy band. The energy bands used for the colors (soft and hard color) and intensity, are given in Table 3. The lower energy boundaries for the soft color and intensity were chosen relatively high in order to avoid to the lowest and least reliable energy channels. By plotting the two colors against each other a color-color diagram (CD) was produced. A hardness-intensity diagram (HID) was produced by plotting the hard color against the intensity. To produce the CDs and HIDs we only used data obtained with those PCUs that (for each gain epoch) were always on. For gain epoch 3 these were PCUs 0, 1 and 2, and for gain epoch 4 PCUs 0 and 2. Due to the different numbers of detectors and the differences in the detector settings we decided to produce the CDs and HIDs separately for the two gain epochs. However, in choosing the energy channels we tried to take channels whose energy boundaries were as close as possible.

Due to the aging processes mentioned earlier, observations with the same source spectrum that are made more than a few weeks apart end up at a different location in the CD. To correct for this effect we analyzed a number of *RXTE/PCA* observations of the Crab pulsar (which is assumed to have a constant spectrum, see also Kuulkers et al. 1994) that were taken around the time of our GX 17+2 observations. For all Crab observations we produced the colors in the same energy bands as we used for GX 17+2. We found that the observed colors of the Crab indeed changed. For each observation we calculated multiplicative scaling factors, for both colors, with respect to those of the first Crab observation. We used these factors to scale the colors of the GX 17+2 observations back to those of the first GX 17+2 observation. This procedure could only be applied to the epoch 3 observations, where, as expected, we found it to result in a narrower track in the CD. No corrections were applied

for the intensity. Since no Crab observations were available for the March 2000 observations, no corrections could be applied to epoch 4 data.

Our power spectral analysis was based on selecting observations as a function of the position along the Z track in the CD. We used a method that is based on the 'rank number' and ' S_z ' parameterization methods introduced by Hasinger et al. (1990) and Hertz et al. (1992), and that has been gradually refined in similar studies (Kuulkers et al. 1994; Kuulkers & van der Klis 1996; Kuulkers et al. 1997; Wijnands et al. 1997b; Dieters & van der Klis 2000). In this method in its current form, all points in the CD are projected onto a bicubic spline (see Press et al. 1992) whose normal points are placed by hand in the middle of the Z track (see Figure 2). The HB/NB and NB/FB vertices are given the values $S_z=1$ and $S_z=2$, respectively. The rest of the Z track is scaled according to the length of the NB. Problems arise when sharp curves are present in the track, in our study most notably around the NB/FB vertex. Due to scatter, points that have FB properties end up on the NB and vice versa. This is not a problem that is only intrinsic to the S_z parameterization; it is a limitation that applies to all selection methods based on colors. No observable parameter, apart from the power spectra, has been identified that could be used to distinguish NB and FB observations around the vertex better than the X-ray colors.

In order to improve on the results of Wijnands et al. (1997a) we wished to combine the epoch 3 and epoch 4 data sets. Unfortunately, the tracks traced out in the CDs for epoch 3 and 4 are not the same and two different splines had to be used for the S_z parameterization. Since the normal points for these splines were drawn by hand, the S_z scales for the epoch 3 and epoch 4 CDs were unlikely to be exactly the same. Therefore, we first transformed the S_z scale of epoch 4 to that of epoch 3. To accomplish this, we measured the frequency of either the HBO or NBO at several places along the Z track of epoch 3, and determined the S_z interval corresponding to the same frequency in the epoch 4 data. The results are shown in Figure 1. We found that $S_{z,epoch4} = (0.06 \pm 0.04) + (1.005 \pm 0.018)S_{z,epoch3}$, showing that, although the scales are the same (within the errors), a small shift is present. We subsequently scaled the S_z values of epoch 4 using the above expression. The above scaling method assumes that the HBO and NBO frequencies are strongly related to S_z . Previous studies of Z sources (see e.g. Kuulkers et al. 1997; Wijnands et al. 1997a; Jonker et al. 2000b; Dieters & van der Klis 2000), as well as the fact that only little scatter is present around the linear relation in Figure 1 seems to confirm this.

Power spectra were created from the data in modes with high time resolution ($\leq 2^{-13}$ s; see Table 2) using standard Fast Fourier Transform techniques (see van der Klis 1989, and references therein). The data were not background subtracted and no dead time corrections were applied prior to the Fourier transformations. We made power spectra in several energy bands, with several frequency resolutions and Nyquist frequencies. We finally settled on 0.0625–4096 Hz power spectra in the 5.1–60 keV (epoch 3) and 5.8–60 keV (epoch 4) bands, since the QPOs were most significantly detected in that band. This choice of frequency range means that the properties of the VLFN, which dominates the power spectrum below 0.1 Hz, could not always be measured satisfactorily, but it does allow to follow the power spectral evolution on time scales down to 16 s. Note that the power spectra of epoch 4 were produced in a slightly higher energy band than those of epoch 3. Due to the gain changes and the limited choice of energy channels this was the best possible

match.

The power spectra were selected on the basis of S_z , as determined from the CD. The S_z selections usually had a width of 0.1 and did not overlap - no power spectrum was represented in more than one S_z -selection. Different widths were used in cases where the power spectrum changed rapidly as a function of S_z (narrower selections) or when the powers were weak (wider selections). All the power spectra in a selection were averaged, and the resulting power spectrum was rms normalized according to a procedure described in van der Klis (1995b).

The properties of the power spectra were quantified by fitting functional forms to them. The low frequency (0.0625–256 Hz) and high frequency (100–4096 Hz) parts of the power spectrum were fitted separately. The high frequency part was fitted with one or two Lorentzians (for the kHz QPOs) and with the function $P(\nu) = P_1 + P_2 \cos(2\pi\nu/\nu_N) + P_3 \cos(4\pi\nu/\nu_N)$ for the dead time modified Poisson level (Zhang 1995; Zhang et al. 1995); no separate term was used for the contribution by the Very Large Events (VLE) count rate since it was absorbed by this fit function. At low frequencies the noise that was present could not be fitted consistently, and varying combinations of functionals had to be used:

- $S_z < 0.0$: A Lorentzian (LFN+VLFN)
- $S_z = 0.0–0.1$: A cut-off power law (LFN+VLFN)
- $S_z = 0.1–1.4$: A power law (VLFN) and a cut-off power law (LFN)
- $S_z = 1.4–1.6$: A power law (VLFN) and a Lorentzian (LFN+NBO)
- $S_z = 1.6–5.0$: A power law (VLFN) and a Lorentzian (LFN)
- $S_z > 5.0$: A power law (VLFN)

The expression for a power law is $P(\nu) \propto \nu^{-\alpha}$, that for a cut-off power law is $P(\nu) \propto \nu^{-\alpha} e^{-\nu/\nu_{cut}}$ (where ν_{cut} is the cut-off frequency), and for a Lorentzian $P(\nu) \propto 1/[(\nu - \nu_c)^2 + (FWHM/2)^2]$ (where ν_c is the centroid frequency and $FWHM$ is the full-width-at-half-maximum). The HBO, its second harmonic and the NBO/FBO were each fitted with a Lorentzian. Below the HBO, at about half its frequency, a broad bump was present that was also fitted with a Lorentzian, whose frequency was sometimes fixed to zero. The dead time modified Poisson level was fitted with a constant.

Note that changes in the fit function, such as using a cut-off power law instead of a Lorentzian or adding an extra component, may lead to changes in the values of other parameters. Errors on the fit parameters were determined using $\Delta\chi^2 = 1$. Upper limits were determined by fixing some or all of the parameters of a component, except the rms amplitude, to values similar to those obtained in the closest S_z selection where it was found to be significant, leaving all other fit parameters free, and using $\Delta\chi^2 = 2.71$ (95% confidence).

A study of the energy dependence and time lag properties of the QPOs and noise components will be presented elsewhere.

3. RESULTS

3.1. Spectral behavior

The CDs and HIDs of both epochs are shown in Figure 2. In both CDs the HB/NB vertex is not well defined, since the

HB is almost a continuation of the NB. This is mainly due to the relatively high energies that we chose for our soft color (see Section 2). At lower energies the turn-over is much clearer. In Figure 3 we show the count rate in several energy bands as a function of S_z , for epoch 4. It shows that the HB/NB vertex in the HID is entirely due to the count rates at low energies. At high energies the HB is a perfect continuation of the NB, and no vertex is present.

In the HID of epoch 3 the Z track appears to be segmented, which was already noted by Wijnands et al. (1997a). Although no corrections for the slow detector aging processes were applied to the intensity in this HID, we note that they would only have made the segmentation more apparent. The shifts in the HID might be due to the secular motion that has been observed in other Z sources. The shifts, of up to $\sim 5\%$ in intensity, do not show up in the CD. This is because colors are ratios of intensities and are therefore not very sensitive to overall intensity changes; exactly for this reason CDs are preferable over HIDs for our purpose. Moreover, the width of the tracks in the CD is about 5%, so changes smaller than this are hard to observe.

The bottom panel of Figure 4 shows the distribution of the time spent by the source in each part of the Z track. The source spent 28% of the time on the HB ($S_z \leq 1$), 44.2% on the NB ($1 < S_z \leq 2$), and 27.8% on the FB ($S_z > 2$). The average speed along the Z track as a function of $S_z(\langle V_z \rangle)$ is shown in the top panel of Figure 4. The speed at a given $S_z(i)$ is defined as $V_z(i) = |S_z(i+1) - S_z(i-1)|/32$ (see also Wijnands et al. 1997b), where i is used to number the points in order of time. As expected the $\langle V_z \rangle$ increases considerably when the source enters the FB, but unexpectedly also at the top of the HB ($S_z < 0.5$). Combined with the small amount of time spent in the upper HB we can conclude that the source reaches to S_z values this low only in brief, quick dashes.

For a more detailed analysis of the spectral changes as a function of the position along the Z track in GX 17+2 we refer to O'Brien et al. (2001, in preparation).

3.2. Power spectra

3.2.1. Low Frequency QPOs and Noise Components

Figure 5 shows the low frequency part (0.0625–256 Hz) of the power spectrum for nine different S_z selections. The power spectra shown in Figure 5 are selected from epoch 3 and epoch 4 and are therefore a combination of 5.1–60 keV and 5.8–60 keV data. The percentage of epoch 3 and epoch 4 data varies between the S_z -selections. The contribution of epoch 3 data is highest at the extremes of the S_z range, reaching 100%, and gradually decreases from both ends to $\sim 10\%$ around $S_z=1$.

Several components can be seen, which change in strength and shape as a function of S_z . The different components are identified in Figure 5 and the S_z ranges in which they were detected are given in Table 4. The component identified as the sub-harmonic of the HBO is rather broad and does not have the appearance of a QPO. However, based on the frequency ratios (see below) it is referred to as the sub-harmonic.

Some difficulties were experienced with fitting the low frequency part of the power spectrum between $S_z=1.4$ and $S_z=1.6$, where two or more components with similar frequencies were simultaneously present. Above $S_z=1.4$ the NBO appeared, as a broad feature on top of the LFN. We were not able to distinguish the two components and decided to fit them together with a single Lorentzian. The fit values are not used in figures and tables, since they do not represent any of the individual

components. Above $S_z=1.6$, the NBO and LFN could be distinguished more easily. The fit function used for the LFN, which was underlying the NBO, was changed to a Lorentzian to be more consistent with fits at higher S_z (fits with a cut-off power law gave equally good χ^2_{red} at this S_z).

In the following sections the results for each of the components will be presented.

3.2.2. HBO

The HBO was detected between $S_z=-0.6$ and $S_z=2.1$ and its second harmonic between $S_z=-0.6$ and $S_z=1.0$. The second and third columns of Figure 6 show their rms amplitudes, FWHM and frequencies as a function of S_z (see also Table 5). The frequency of the HBO increased from 21.3 Hz at $S_z=-0.43$ to 60.3 Hz at $S_z=1.45$ and then decreased to 48.5 Hz at $S_z=2.04$. The second harmonic of the HBO had a frequency that was on average 1.941 ± 0.007 times that of the first harmonic, which is significantly different from the expected value of 2. A likely explanation for this discrepancy is proposed in Section 4.1.1. Between $S_z=-0.6$ and $S_z=1.0$ both the HBO and its second harmonic decreased in strength, with the decrease of the second harmonic occurring somewhat faster than that of the HBO. In that same S_z interval the FWHM of the HBO and its second harmonic were fairly constant (showing a slight increase), although considerable scatter was present around the average values (which were, respectively, 7.9 ± 0.3 Hz and 14.4 ± 0.6 Hz). The Q values of the HBO and its harmonic are shown in Figure 7. In the S_z range where both were detected their Q values were consistent with each other. When the second harmonic was not significantly detected anymore ($S_z > 1.0$) the rms amplitude and the FWHM of the HBO both decreased from, respectively, $2.45 \pm 0.08\%$ and 9.7 ± 7 Hz ($S_z=0.5$ –1.0) to $1.48 \pm 0.06\%$ and 5.1 ± 0.4 Hz ($S_z=1.0$ –1.5). Between $S_z=1.0$ and $S_z=1.5$ the relation between the S_z and the HBO frequency started to flatten. Above $S_z=1.5$ the frequency of the HBO clearly dropped, initially quite abruptly and later on more smoothly. This frequency drop coincided with an increase in the FWHM to 15.7 ± 1.5 ($S_z=1.5$ –2.1); the rms amplitude showed a small increase to $2.1 \pm 0.1\%$ ($S_z=1.76$), followed by a decrease to $1.2 \pm 0.2\%$ ($S_z=2.04$).

Underlying the HBO and its second harmonic, but with a central frequency lower than that of the HBO, we found a broad feature that was also fitted with a Lorentzian. It was significantly detected between $S_z=-0.6$ and $S_z=1.3$. The properties of the broad feature are shown in the first column of Figure 6 (see also Table 5). Below $S_z=0$ the frequency of the Lorentzian was fixed to zero. Between $S_z=0.5$ and $S_z=1.5$ the frequency of the broad feature is on average 0.539 ± 0.015 times that of the HBO. This suggests that the broad feature is the sub-harmonic of the HBO, certainly when one takes into account that the frequency of a broad feature is rather sensitive to the shape of the continuum. Whereas the rms amplitude and the frequency of the sub-harmonic both change strongly with S_z the FWHM remains more or less constant, with an average value of 29.5 ± 1.5 Hz.

3.2.3. NBO and FBO

The NBO and FBO were detected between $S_z=1.6$ and $S_z=2.7$. The fit results for the NBO/FBO are shown in Figure 8 (see also Table 5). Below $S_z=2.1$ the NBO (represented by the filled circles in Figure 8) has a fairly constant frequency, with values between 6.3 Hz and 7.0 Hz. Its rms amplitude increases

from 1.7% to 3.2%, and the FWHM is approximately ~ 2.1 or ~ 3.8 . In the $S_z=2.0\text{--}2.1$ selection both the NBO and FBO were present. This is likely an artifact of the S_z selection method, since a careful inspection of dynamical power spectra showed no evidence for simultaneous presence of both QPOs. It is interesting to note though, that in the $S_z=2.0\text{--}2.1$ selection the frequency of the FBO is 2.0 ± 0.1 times that of the NBO, which could mean that the two NBO and FBO are harmonically related (however, see below). The FBO increased in frequency from 13.9 Hz ($S_z=2.04$) to 23.1 Hz ($S_z=2.65$), while its FWHM increased from ~ 5 Hz to ~ 13 Hz. The rms amplitude of the FBO initially continued the trend of the NBO rms amplitude; it increased from 2.8% ($S_z=2.04$) to 5.6% ($S_z=2.23$), but then decreased to 1.8% ($S_z=2.65$).

To study the transitions between the NBO and FBO more carefully, we inspected all dynamical power spectra of observations with S_z values around 2. Although no clear transitions were found, mainly due to the limited quality of the dynamical power spectra, we did in some cases see QPOs with intermediate frequencies (~ 10 Hz), suggesting that the frequency does not jump directly from ~ 7 Hz to ~ 14 Hz. Fitting the power spectra in consecutive time intervals (longer than 16 s), rather than inspecting dynamical power spectra with the eye, will probably lead to more conclusive results, but is beyond the scope of the current paper. The time scales on which the NBO/FBO frequency changed from ~ 7 Hz to ~ 14 Hz and back were as short as a few tens of seconds.

We also studied the behavior of the NBO/FBO during two long type I X-ray bursts. The first one started on 1998 November 18 at 08:51:26 UTC, the second one on 1999 Oct 10 at 09:10:47 UTC. Their exponential decay times were, respectively, 189 ± 2 s and 144 ± 2 s (Kuulkers 2001). Both bursts occurred near the NB/FB vertex and in the power spectra of their respective observations the NBO/FBO is clearly detected. No other QPOs were detected in the power spectra of these bursts. Figure 9 shows the dynamical power spectra of both bursts, together with their 2–60 keV light curves. During the brightest part of the bursts the NBO/FBO seemed to disappear. Apparently, the burst flux was not modulated at the NBO/FBO frequencies with the same amplitude as the persistent flux. To quantify this, we determined upper limits on the NBO/FBO strength and compared those with the values outside the bursts. The results are shown in Table 6. Clearly, during the brightest part of the bursts the rms amplitude of the NBO/FBO was significantly weaker, not only as a fraction of the total flux, but also in absolute terms (and hence as a fraction of the persistent flux, if the persistent emission is assumed to continue during the bursts). These measurements constitute the first determination of the effect of X-ray bursts on the NBO/FBO. The fact that the burst suppresses the QPO can have important consequences for our understanding of its formation mechanism (see Section 4.1.4).

3.2.4. Noise components: LFN and VLFN

LFN was detected between $S_z=-0.6$ and $S_z=5.0$. As mentioned before, the appearance of the NBO around $S_z=1.5$, kept us from putting firm constraints on the LFN parameters between $S_z=1.4$ and $S_z=1.6$. The fit results for the LFN are shown in Figure 10 (see also Table 7), in two separate columns: one for the fits with a cut-off power law fit ($S_z=0.0\text{--}1.4$) and one for the fits with a Lorentzian ($S_z<0.0$ and $S_z=1.6\text{--}5.0$). The strength of the LFN was in both cases defined as the integrated power

spectral density between 1 Hz and 100 Hz. We note that below $S_z=0.1$ the VLFN was not fitted separately from the LFN. An inspection of 1/256–4096 Hz power spectra below $S_z=0.1$ showed that a weak power law component was present at frequencies below 0.1 Hz. This component was probably VLFN; its power in the 1–100 Hz range was much smaller than that of the LFN, so, although some VLFN power was absorbed by the LFN, this did not affect the LFN rms amplitudes significantly. The strength of the LFN changed considerably as a function of S_z . It showed a narrow peak between $S_z=-0.6$ and $S_z=0.2$ of $\sim 5\%$ rms. Between $S_z=0.2$ and $S_z=1.7$ it gradually decreased from $\sim 4.5\%$ rms to $\sim 2.5\%$ rms. Another decrease was observed between $S_z=2.7$ and $S_z=5.0$, from $\sim 3.8\%$ rms to $\sim 0.9\%$ rms. The behavior between $S_z=1.7$ and $S_z=2.7$ was quite erratic, probably due to interactions with the fit functions of NBO and FBO.

The centroid frequency of a Lorentzian and the cut-off frequency of a cut-off power law cannot be directly compared. Since we wanted to see how the typical frequency of the LFN evolved with S_z , we chose to plot ν_{max} , which is the maximum in a $\nu P(\nu)$ plot and the frequency at which most of the power is concentrated per logarithmic frequency interval (Belloni, Psaltis, & van der Klis 2001, in prep.). For a Lorentzian ν_{max} is $(\nu_c^2 + (FWHM/2)^2)^{1/2}$ and for a cut-off power law ν_{max} is $(1-\alpha)\nu_{cut}$ (see Section 2 for analytical expressions for a Lorentzian and cut-off power law). As can be seen from Figure 10, between $S_z=-0.6$ and $S_z=1.7$ ν_{max} smoothly increased from ~ 1.2 Hz to ~ 14.7 Hz. Above $S_z=1.7$ the errors on ν_{max} were larger and the behavior was less clear. Between $S_z=1.7$ and $S_z=2.3$ ν_{max} decreased to ~ 6.5 Hz, and above $S_z=2.3$ it increased again to ~ 15 Hz. We tested whether the change of the fit functions at $S_z=0.0$ affected the values for ν_{max} and the other power spectral parameters, by swapping the fit functions used below and above $S_z=0.0$; no significant changes were found.

VLFN was detected over almost the whole S_z range. Although we only started fitting the VLFN separately from the LFN above $S_z=0.1$ (in the 16 s power spectra), VLFN was present at frequencies below 0.1 Hz in the 256 s power spectra below $S_z=0.1$. In the 16 s power spectra it was only significantly detected above $S_z=0.3$. The fit results for the VLFN are shown in Figure 11 (see also Table 7). Between $S_z=0.3$ and $S_z=1.4$ the VLFN strength decreased from $\sim 0.9\%$ rms to $\sim 0.4\%$ rms. Above $S_z=1.4$ its strength increased, to a peak value of $\sim 1.3\%$ rms at the NB/FB vertex. On the lower FB the strength decreased again, to a value of $\sim 0.5\%$ rms, and above $S_z=3.0$ it increases to $\sim 1.6\%$ rms at the top of the FB. The index of the VLFN slowly increased from ~ 0.6 to ~ 1.0 between $S_z=0.1$ and $S_z=2.4$, with a small peak between $S_z=1.6$ and $S_z=1.9$, where the index had a value of ~ 1.5 . Between $S_z=2.4$ and $S_z=3.2$ the VLFN was much steeper. The indices were not well constrained and had values between 1.7 and 4.0. Above $S_z=3.2$, where the error bars are much smaller, the index slowly decreased from 2.1 to 1.8.

3.3. High Frequency QPOs

Both the lower and upper kHz QPO were clearly detected; the lower kHz QPO between $S_z=0.5$ and $S_z=1.5$, the upper kHz QPO between $S_z=-0.3$ and $S_z=1.7$. The results can be found in Table 8 and are shown in Figure 12. The QPO frequencies showed a clear increase with S_z , although both relations flattened at their low frequency ends. The FWHM of the lower kHz QPO was consistent with being constant at ~ 100 Hz, whereas

the rms amplitude showed a peak near $S_z=1.05$ with a value of 3.6 ± 0.3 . The rms amplitude and FWHM of the upper kHz QPO both decreased with S_z .

Figure 13a shows the frequency difference of the two kHz QPOs as a function of the frequency of the upper kHz QPO. Some fits were made to the data; they are also shown in Figure 13a. The best fit to the frequency difference with a constant gave a value of 282 ± 4 Hz. The $\chi^2/d.o.f.$ for this fit was $18.6/9$, which means that at a 97% confidence level the frequency difference was not constant. This is the first time that this is observed for GX 17+2. Fits with first and second order polynomials (taking into account errors in both coordinates) resulted in, respectively, $\chi^2/d.o.f.=15.0/8$ and $\chi^2/d.o.f.=3.7/7$. Although the latter two fits show that with 99.76 % confidence (3.2σ) a decrease towards higher frequency is not monotonic, it is not clear either whether the decrease towards lower frequencies is significant or not. This would be the first time that such a decrease towards lower frequencies is observed in any kHz QPO source with a non-constant frequency difference. To test this two fits with a broken line (not shown) were performed, where in one case the slope of the low frequency part was fixed to zero. They resulted in $\chi^2/d.o.f.=6.28/7$ (slope fixed) and $\chi^2/d.o.f.=2.52/6$ (slope free), which suggests that the frequency decrease towards lower frequency is only significant at a 97.6% confidence level (2.4σ).

In Figure 13b we plot the curves produced by Stella & Vietri (1999) for the frequency separation as a function of the upper kHz QPO frequency. For comparison we also plotted the data for Sco X-1 from van der Klis et al. (1997b). Clearly, the decrease of the frequency difference towards lower frequencies, which occurs in a frequency range for the upper kHz QPO that was not observed in Sco X-1, does not fit the theoretical curves.

The Q values (frequency/FWHM) of the two kHz QPOs were consistent with each other and with that of the HBO and its harmonic (see Figure 7); between $S_z=0.5$ and $S_z=1.5$ they all increased from ~ 5 to ~ 10 . This unexpected finding may provide a key to understanding the formation mechanism of the three QPOs - this will be further discussed in Section 4.1.3.

When comparing Figures 12 and 6 one can see that above $S_z=1.5$, where the HBO frequency starts to decrease, the upper kHz QPO frequency still increases. In Figure 14 we plot the frequencies of both QPOs against each other. For values of the upper kHz frequency lower than 1030 Hz the frequencies are well correlated, but above there is a clear anti-correlation. The solid line is the best power law fit to the points below 1000 Hz. The power law index is 2.08 ± 0.07 . This is the first time in any source showing kHz QPOs that an anti-correlation is observed between the frequencies of the low and high frequency QPOs (see Section 4.1.1 for a discussion).

4. DISCUSSION

We performed a detailed study of the low and high frequency power spectral features of the neutron star low-mass X-ray binary and Z source GX 17+2. As was found in previous studies of GX 17+2 and other Z sources, the properties of most power spectral features correlated well with the position of the source along the Z track in the X-ray color-color diagram. Some new results were found, the most interesting being the fact that the frequency separation of the kHz QPOs was not constant and probably not monotonic (Fig. 13), that their Q values were consistent with those of the HBO and its harmonic (Fig. 7), and that the frequency of the upper kHz QPO anti-correlated

with that of the HBO when the latter started to decline on the NB (Fig 14). We also found a sub-harmonic of the HBO and showed that the NBO/FBO amplitude is suppressed during type I X-ray burst (Fig. 9). These findings contribute significantly to an understanding of the processes that occur in inner regions of accretion disk in neutron star LMXBs. In the remainder of this section they will be discussed in more detail.

4.1. Timing behavior

4.1.1. Horizontal Branch Oscillations

The HBO of GX 17+2 and its second harmonic were discovered with *EXOSAT* (Stella et al. 1985, 1987; Langmeier et al. 1990). Kuulkers et al. (1997) studied the power spectra of GX 17+2 in terms of S_z , and found the HBO between $S_z=0.0$ and $S_z=0.3$, with a frequency of 24.0–27.3 Hz. Note that the S_z scale from Kuulkers et al. (1997) is not necessarily exactly the same as ours, due to uncertainties involved in the S_z method (see Section 2). With *Ginga* the HBO was found between 19.5 and 31.2 Hz (Penninx et al. 1990); no S_z range was determined, but from the CD and HID it was clear that it was only detected on the HB. Both in the *EXOSAT* and *Ginga* data the frequency and FWHM ratios of the second and first HBO harmonics are consistent with 2, but also with the values that we found, i.e. a frequency ratio 1.941 ± 0.007 and a FWHM ratio of 1.84 ± 0.07 . Using *RXTE* data from February 1996, that were not included in our analysis (see Section 2), Wijnands et al. (1996) observed the HBO for the first time on the NB. Not only were the frequencies much higher (~ 50 –62 Hz) than found before on the HB, but they also decreased significantly above $S_z=1.4$. This decrease, again above $S_z=1.4$, was confirmed by Wijnands et al. (1997b) using the 1997 *RXTE*/PCA data, that were also part of our current data set. In our data the decrease of the HBO frequency started only above $S_z=1.5$. This discrepancy is likely due to the fact that the HB/NB vertex was not (well) observed in the CDs used by Wijnands et al. (1996) and Wijnands et al. (1997b), so the S_z scale could not be determined as well as in our case.

There were interesting features in the HBO properties which reproduced between the 1996 *RXTE* data and our *RXTE* data. In both cases the S_z dependence of the HBO frequency was not symmetric around its peak value. Below, the frequency slowly flattened off to its maximum value, but above it showed a fast decrease by a few Hz that was followed by a more or less linear decrease with S_z . Simultaneously with the frequency drop, the FWHM increased by more than a factor two. The flattening of the HBO frequency in our data set started around $S_z=1.0$, at the same point where the HBO harmonic became undetectable and the FWHM of the HBO decreased by a factor of about two. Note that these sudden changes in the HBO properties do not coincide with changes in the fit function that was used or with sudden changes in the other low frequency components.

We compared our results with *RXTE* studies of the Z sources GX 5-1 (Wijnands et al. 1998a), Cyg X-2 (Wijnands et al. 1998b) and GX 340+0 (Jonker et al. 2000b). The HBO frequency in Cyg X-2 decreased above $S_z=1.1$, although it was also consistent with remaining constant (see also Wijnands et al. (1997b), for an analysis based on *Ginga* data, where a similar decrease is reported). As the decrease started, the FWHM increased by a factor almost two, similar to what we observed in GX 17+2. In GX 340+0 the HBO frequency showed a strong flattening above $S_z=1$, but the behavior of the FWHM was not well defined above that point. It is interesting to note

though, that the flattening of the frequency- S_z relation started around the S_z where the harmonic of the HBO became undetectable ($S_z=0.9$). In GX 5-1 only weak flattening was observed in the frequency, which like in GX 17+2 and GX 340+0 started around the S_z where the harmonic of the HBO became undetectable ($S_z=1.0$). When it disappeared the FWHM of the HBO increased, opposite to what we observe in GX 17+2. In all sources the rms amplitude of the HBO decreased with S_z , although both Cyg X-2 and GX 17+2 show a small increase around the S_z where the frequency drop started.

A possible explanation for the frequency decrease of the HBO above $S_z=1.5$ was put forward by Wijnands et al. (1996). Based on the two-flow (disk flow + radial flow) accretion model described in Fortner et al. (1989), they suggested that, although the total mass accretion rate onto the neutron star increases from the HB/NB vertex to the NB/FB vertex, the mass accretion rate through the thin disk actually decreases above $S_z=1.5$. This decrease is then compensated for by a faster increase in the radial or spherical inflow. Since the HBO frequency is set by the disk flow (in the framework in which they discussed the HBO), a decrease in the accretion rate through the disk above $S_z=1.5$ would then automatically lead to a decrease in frequency. This model also naturally explains the appearance of the NBO around $S_z=1.5$, which is strongly connected to the strength of the radial flow (Fortner et al. 1989). A difficulty with this explanation is that there is no spectral evidence for a change in the accretion flow geometry around $S_z=1.5$. A possible solution for this is that this change is gradual and starts already before $S_z=1.5$. The onset of the change in the flow geometry might for instance show up as the HB/NB vertex. The increase in the disk flow would then get less until $S_z=1.5$, above which it decreases. Since this is a gradual process, no sudden spectral changes at $S_z=1.5$ are expected. Another possible explanation for the frequency decrease of the HBO, which is also related to the appearance of the NBO, might lie in the increase of the radiation pressure. This could reduce the effective gravity and thereby also the HBO frequency. However, the kHz QPO frequencies would also have to be affected by this, which seems not to be the case. A more promising explanation is offered by Morsink & Stella (1999) who show that the decrease can be explained by their model for the kHz QPOs and HBO. This will be discussed at the end of this section.

Harmonics of the HBO have been found in all Z sources where the HBO has been observed. In GX 5-1, Cyg X-2 (Wijnands et al. 1997b) and GX 340+0, the frequency ratio of the (second) harmonic and the fundamental (=first harmonic) is generally less than two, similar to what we found in GX 17+2. This can be explained, at least in GX 17+2, by looking at the S_z dependence of the rms amplitudes of both components. From Figure 6 it is clear that the S_z dependence of the rms amplitude of the HBO harmonic is steeper than that of the HBO fundamental. Although in a certain S_z selection both frequencies will tend to be dominated by those with the higher rms amplitudes, and hence by lower S_z and lower frequencies, this effect will be stronger for the harmonic than for the fundamental, since the S_z dependence of its rms amplitude is steeper. The result is that in general the frequency ratio will end up to be less than two. To test this hypothesis we calculated the weighted averages of two harmonically related linear functions, representing the HBO- S_z relation between $S_z=0.0$ and $S_z=1.0$. As weight we used linear functions that were fit to the rms- S_z relation between $S_z=0.0$ and $S_z=1.0$. The ratio of the weighted averages was 1.93,

which is very close to the observed value of 1.94.

Peaked features with frequencies intermediate to those of the LFN and the HBO have been reported for GX 340+0 (Jonker et al. 2000b), Sco X-1 (van der Klis et al. 1997b; Wijnands & van der Klis 1999a), GX 5-1 (not well measured, Kuulkers et al. 1994, but see P. Jonker et al. 2001, in preparation), and now also for GX 17+2. Based on the average frequency ratio of this sub-HBO component and the HBO in GX 17+2, 0.539 ± 0.015 , we suggest that, similar to what was suggested for GX 340+0, it may be the sub-harmonic of the HBO. In GX 340+0 this ratio was ~ 0.45 , but it was consistent with 0.5 (P. Jonker, priv. comm.). In Sco X-1 the sub-HBO peak was not fitted with a Lorentzian, but with a broken power law whose break frequency was 0.6–0.7 times the frequency of the HBO (Wijnands & van der Klis 1999a). These values are not consistent with 0.5 (R. Wijnands, priv. comm.); fits with Lorentzians would probably have resulted in values closer to 0.5. It was suggested (van der Klis et al. 1997b) that it could possibly be the true signature of the noise component that is expected to accompany HBOs (Lamb et al. 1985) or that it might be the band limited noise component seen in atoll sources and BHs (Wijnands & van der Klis 1999a). In all three cases the sub-HBO component appeared as a broad feature, unlike the HBO and its second harmonic. If it were really harmonically related to the HBO, technically it should be called the fundamental, and the HBO and its harmonic should then be referred to as the second and fourth harmonic. However, to stay consistent with other studies we will use the terms sub-harmonic, fundamental and second harmonic.

A comparative study by Wijnands & van der Klis (1999a) of low frequency (HBO-like) QPOs and band limited noise components in the neutron star Z and atoll sources and black holes revealed strong correlations between the typical frequencies of those components. When plotting the frequency of the low frequency QPO versus the break frequency of the band limited noise they found that the branch traced out by the Z sources, although lying parallel to that of the atoll source and black holes, was slightly offset. It is interesting to see that this discrepancy between the Z sources on the one hand and the atoll sources and black holes on the other disappears (Jonker et al. 2000b), at least for GX 17+2, Sco X-1 and GX 340+0, when one uses the frequencies of the sub-HBO component, instead of HBO frequency (see also Wijnands & van der Klis 1999a). If the low frequency QPO in the atoll sources and the sub-HBO component of the three Z sources would indeed be the same QPO, this would mean that the Z sources do not anymore follow the relation between the low frequency (HBO-like) QPO and the lower kHz QPO as defined by atoll and black hole systems (Psaltis et al. 1999). It is interesting to see that the three Z sources would then end up near or slightly above a second relation that is traced out by atoll sources like 4U 1728-34 and 4U 1608-52. At the moment, however, it seems that the relation found by Wijnands & van der Klis (1999a) and the main relation of Psaltis et al. (1999) are mutually exclusive for the two types of sources. Note that Wijnands & van der Klis (1999a) found that if in their plot for Sco X-1 the frequencies of the sub-HBO component and the HBO were used, instead of the LFN and HBO frequencies, the discrepancy between Sco X-1 and the non-Z sources also disappeared. This reinterpretation has the advantage of preserving the consistency with the Psaltis et al. (1999) relation as well.

The dominance of the even harmonics over the odd harmon-

ics in the low frequency (HBO-like) QPOs, as suggested by the presence of a sub-harmonic of the HBO, is not only observed in the Z sources, but also a common feature in BHCs such as GS 1124–68 (Belloni et al. 1997) and XTE J1550–564 (Homan et al. 2001). It suggests that a two-fold symmetry is present in the production mechanism of these low frequency QPOs. In the case of neutron stars it could be explained by an asymmetry in the magnetic field, which results in different areas for the polar caps (see e.g. Kuulkers et al. 1997). However, this assumes that the magnetic field and polar caps are involved in the QPO mechanism, and is therefore not applicable to BHCs. A more appealing model would be one in which the QPOs are produced in the disk, and do not require the presence of a solid surface or magnetic field, such as the relativistic precession model (Stella & Vietri 1998, see below), in which a two-fold symmetry is introduced by the two points at which the slightly inclined orbits of blobs of matter cross the plane of the accretion disk.

Several models have been proposed for the HBO. In the magnetospheric beat frequency model (Alpar & Shaham 1985; Lamb et al. 1985), which was developed soon after the discovery of the HBO in GX 5-1 (van der Klis et al. 1985), its frequency is the beat between the neutron star spin frequency and the orbital frequency of blobs of matter around the neutron star. This model for the HBO prevailed until the discovery of the kHz phenomena in the neutron star LMXBs (Strohmayer et al. 1996; van der Klis et al. 1996; van der Klis 2000, for a review), when it was suggested as an explanation for the similarity of the kHz QPO frequency separation and the frequency of the burst oscillations in 4U 1728–34 (Strohmayer et al. 1996; Cui 2000; Campana 2000). The sonic point beat frequency model (Miller, Lamb, & Psaltis 1998) explains the frequencies of the kHz QPOs in terms of another beat frequency model. While the HBO is proposed to be explained by the original model, it is assumed that a Keplerian disk still exists within the magnetosphere. The observed kHz frequencies are close to the orbital frequency at the sonic point of this disk and the beat of this frequency with neutron star spin frequency. The model requires the presence of a magnetosphere and a solid surface, and can therefore not explain the low and high frequency QPO in the black hole candidates. More recently relativistic precession models have been proposed for the HBO. (Stella & Vietri 1998, 1999; Morsink & Stella 1999; Stella et al. 1999 however see Markovic & Lamb 2001). Three frequencies are predicted, corresponding to the three fundamental frequencies of the motion of a test particle in the vicinity of a compact object, which are identified with the HBO and the two kHz QPOs. However, the lowest predicted frequency, which should explain the HBO, is a factor 2 lower than the low frequency QPOs in the atoll sources and the sub-harmonic of the HBO in the Z sources. Hence, a mechanism to produce second harmonics is required. Stella & Vietri (1998) suggested that a modulation at twice the precession frequency might be generated at the two points where the inclined orbit of a blob intersects the disk.

A principal aim of our observing campaign in 1999 was to check on the relation between HBO frequency (whose increase was known to turn into a decrease towards higher S_z) and upper kHz QPO frequency. The present analysis shows that this aim was reached. Clearly, a decrease, or even flattening, of the upper kHz QPO frequency, is not observed to accompany the decrease in HBO frequency (see Figure 14). While below a kHz QPO frequency of 1030 Hz it is correlated to the HBO frequency, above 1030 Hz the two frequencies are anti-

correlated. In a pure relativistic precession model, this can not be explained. However, if classical precession due to oblateness of the neutron star also plays a role, such an explanation is possible. For certain combinations of neutron star parameters, the prediction is that above a certain value of the upper kHz QPO frequency, the frequency of the HBO does in fact starts to decrease (see Morsink & Stella 1999), due to the increasing importance of the classical precession that is related to the stellar oblateness. In GX 17+2 this turn-over of the HBO frequency occurs at a value of ~ 1 kHz for the upper kHz QPO with a peak frequency of ~ 60 Hz for the HBO. Judging from Figure 2 in Morsink & Stella (1999), the relation between the HBO and upper kHz QPO frequencies in GX 17+2 would require a high neutron star spin frequency (~ 500 –700 Hz), a neutron star mass of more than $2 M_\odot$, and a hard equation of state (assuming the observed HBO frequency is four times the predicted frequency). In the relativistic precession model, well below the turn-over, the HBO frequency is expected to scale quadratically with the upper kHz QPO frequency. The best power law fit to the data below 1000 Hz yielded an index of 2.08 ± 0.07 (see Figure 14), which is consistent with a quadratic relation. Unlike in the sonic point beat frequency model no actual mechanism is proposed for the production of QPOs. However, in a recent model by Psaltis & Norman (2001) the accretion disk acts as low band-pass filter with resonances close to the three frequencies predicted in the relativistic precession model. It is unclear to what extent the details of the relativistic precession model (i.e. the turnover in the relation between HBO and upper kHz frequency) carry over to the Psaltis & Norman (2001) description.

In the sonic point beat frequency model a turnover in the HBO-upper kHz QPO relation is not predicted, but as the two frequencies do not directly depend on each other, the model is flexible enough to account for it; if the turnover in HBO frequency is explained by the two flow model put forward by Wijnands et al. (1996), the steady increase of the upper kHz QPO frequency can in principle be explained by assuming that most of the radial flow falls back to the disk and rejoins the disk flow before the sonic point is reached, so that \dot{M} there, and hence the upper kHz QPO frequency keep increasing.

4.1.2. High frequency QPOs

The kHz QPOs in Z sources (van der Klis et al. 1996; Wijnands et al. 1997a, 1998a; Jonker et al. 1998; Wijnands et al. 1998b; Zhang et al. 1998, see van der Klis 2000 for a review) have been found on the HB and NB (and in Sco X-1 also on the FB), with the S_z range in GX 17+2 being the largest. In general the upper peak in the Z sources is detected over a larger S_z range than the lower peak. The strength of the upper peak shows a clear dependence on S_z ; rms amplitudes in the upper HB are about 5–6% (in energy bands above ~ 5 –7 keV) and they smoothly decrease to values of 1–2% on the lower NB. The lower peak is usually a bit weaker, and its strength is fairly constant. The FWHM of the lower peak is also quite constant, whereas that of the upper peak usually decreases with S_z . Both peaks therefore become more coherent with increasing S_z , but this effect is stronger in the upper peak. The lower peak has been found between frequencies of 215 Hz and 845 Hz; the upper peak between 505 Hz and 1130 Hz. The frequency separation of the two peaks was found to decrease in Sco X-1 when the frequency of the QPOs increased (van der Klis et al. 1997b). In the other Z sources it was found (Wijnands et al. 1997a;

Jonker et al. 1998; Psaltis et al. 1998) that the frequency separation was both consistent with the behavior of Sco X-1 and with being constant. No burst oscillations have been found in the two bursting Z sources GX 17+2 (Kuulkers et al. 1997; Kuulkers 2001) and Cyg X-2 (Kuulkers et al. 1995; Wijnands et al. 1998a; Smale 1998).

Our findings of the kHz QPOs in GX 17+2 are compatible with the general properties given above. The kHz QPOs in GX 17+2 were discovered with *RXTE* (van der Klis et al. 1997a; Wijnands et al. 1997a). In our data the lower kHz QPO was found between 517 Hz and 794 Hz ($S_z=0.5-1.5$) and the upper kHz QPO between 618 Hz and 1087 Hz ($S_z=-0.3-1.7$), similar to what was reported by Wijnands et al. (1997a).

An important new result is that the frequency difference is no longer consistent (at a 97% confidence level) with being constant (see Figure 13). The frequency separation reached a maximum value of 308 Hz, when the upper peak frequency was about 915 Hz, and fell off in both directions to values of 263 Hz and 239 Hz, when the frequencies of the upper peak were, respectively, 780 Hz and 1033 Hz. Note that the decrease in both directions, when fitted with a parabola, resulted in significantly (3.1σ) better fits than that with a constant. The decrease in the frequency separation at the low frequency side of the upper kHz QPO, although itself only significant at a 2.3σ level, has not been seen before in any kHz QPO source. In the other LMXBs that show an non-constant frequency separation, Sco X-1 (van der Klis et al. 1997b), 4U 1608–52 (Méndez et al. 1998a,b), 4U 1735–44 (Ford et al. 1998b), and 4U 1728–34 (Méndez & van der Klis 1999), the frequency separation was not measured at upper peak frequencies as low as in GX 17+2. Although both the sonic point beat frequency model (Miller et al. 1998; Lamb & Miller 2001) and the relativistic precession model (Stella & Vietri 1998, 1999; Stella et al. 1999) are capable of explaining the observed decrease in frequency difference towards higher upper peak frequencies, they have severe problems with a decrease towards lower frequencies. In the relativistic precession model such a decrease is in principle expected, but not as sharp as we observed (Stella & Vietri 1999, see also Figure 13). The sonic point beat frequency model can apparently not account for it at all (Lamb & Miller 2001).

As discussed above (at the end of Section 4.1.1), the relativistic precession model can for certain combinations of neutron star parameters explain the observed anti-correlation between the HBO and the upper kHz QPO by the effect of classical precession (Morsink & Stella 1999). In the sonic point beat frequency model the HBO and kHz QPO are not produced by the same mechanism, so their frequencies do not necessarily need to be correlated at all times. However, an anti-correlation is not predicted.

We note that recent investigations of the relativistic precession model by Markovic & Lamb (2001) have cast some doubt on the frequencies predicted by that model and relations between them.

4.1.3. *Q* values of the HBO and kHz QPOs

The Q values of the kHz QPOs are remarkably similar to each other, and to those of the HBO and its harmonic (see Figure 7). They also show an almost simultaneous increase above $S_z=1$. If the QPOs were artificially broadened by our selection method, averaging together peaks with different centroid frequencies, one would expect correlations of the FWHM with the width of the S_z selection and with $d\nu/dS_z$. Such correlations, if present

at all, are far too weak to explain the observed similarities.

The FWHM of a QPO can be caused by several mechanisms. Intrinsic frequency variations, phase jumps, the simultaneous presence of several frequencies, and a finite lifetime of the signal will all cause a signal to appear as a broadened peak in a power spectrum. The data quality did not allow us to test the phase jump option. Lifetime broadening can probably not explain our data. In the sonic point beat frequency model there is no reason why the lifetimes of the low and high frequency oscillations, which are determined by different processes, would lead to similar Q values. In the relativistic precession model, where all frequencies are generated by a single blob of matter, the lifetime for all variations should to first order be the same. However, in that case the Q values of the kHz QPOs should be much higher (by a factor 10–20) than those of the HBO, since more kHz cycles fit in a blob's lifetime. Of course, it is possible that the lifetime of the oscillations is not determined by the lifetime of the blob, but rather by a damping factor. Assuming that these factors are not the same for the different QPOs, the similarity of the Q values could in principle be explained. This is a rather unlikely possibility though, since there is no obvious reason why the (independent) damping factors would be fine tuned in a such a way that they lead to similar Q values.

Explaining the Q values by broadening due to the presence of several frequencies does not work either. Below the turnover in the HBO-upper kHz QPO frequency relation the frequency of the HBO scales quadratically with the frequency of the upper kHz QPO. A given range of upper kHz frequencies would therefore lead to a Q value for the HBO that is half the Q value for the upper kHz QPO. This is not consistent with what we find.

Frequency modulation could in principle explain the similar Q values, but only if the modulation is caused by a different parameter than the one that determines the frequency changes along the Z track. Frequency modulation only produces similar Q values if the QPO frequencies vary with the modulating parameter by the same factor, i.e., proportionally to each other. The observed quadratic relation between the HBO frequency and that of the upper kHz QPO as well as the subsequent turnover, shows that this is not the case for the parameter that causes the motion along the Z track. Since we do not even know what the parameter is that causes changes along the Z (see Section 4.2), we have no idea what could be a possible additional mechanism. However, assuming there is one, we discuss the possibility of frequency modulation in a bit more detail. In order for the broadening due to frequency modulation to be observable in our power spectra, the time scale of these variations should be longer than that of the HBO. Assuming that the parameter that causes the frequency modulations also causes some changes in the count rate we could try to identify it in the power spectrum. The only reasonably strong components that we see in our power spectra and whose typical frequencies fulfill the above requirement ($\nu < 10$) are the VLFN, the LFN and the NBO/FBO. The VFLN might be associated with the motion along the Z (see Section 4.1.5); disentangling that effect from a possible additional one on QPO frequencies is beyond the scope of this work. In the S_z range below 1.5 the LFN is of also interest. The strength of the LFN is rather constant below $S_z=1.0$ and decreases rapidly above it. This is in qualitative agreement with the Q values below $S_z=1.5$, which are rather constant up to $S_z=1.0$ and then rapidly increase. Above $S_z=1.5$ the Q values decrease again to a value between 2 and 5.

In that case the broadening might be due to the appearance of the NBO/FBO and the increase in the LFN strength. It is interesting to note that in Sco X-1 it has been found that the kHz QPO properties are clearly modulated by the NBO (Yu et al. 2001). Although the frequency changes they observed seem too small to explain our observed Q values, this may be due to their selection method. In the atoll sources 4U 0614+09 (van Straaten et al. 2000) and 4U 1728-34 (di Salvo et al. 2001) the Q values are also anti-correlated with the strength of the band limited noise. However, comparing the atoll sources 4U 1705-44 (Ford et al. 1998a) and 4U 1735-44 (Wijnands et al. 1998c) with each other, shows that stronger noise does not necessarily mean lower Q values.

4.1.4. Normal and flaring branch oscillations

For the first time we were able to study the properties of the NBO/FBO during type I X-ray bursts. We found that the absolute rms amplitude significantly decreased when the radiation from the neutron star surface increased. This is clearly different from the behavior of the ~ 1 Hz QPOs in the dipping LMXBs 4U 1323-62 (Jonker et al. 1999), EXO 0748-676 (Homan et al. 1999), and 4U 1746-37 (Jonker et al. 2000a), whose absolute rms amplitudes increased during type I X-ray bursts. It is thought that these QPOs are not related to the NBO/FBO in the Z sources. The behavior of the NBO/FBO in GX 17+2 shows that NBO/FBO mechanism is very sensitive to the radiation field. In the framework of a radiation feedback mechanism (see below) it is easy to understand that the NBO disappears during bursts: it is usually only observed in a narrow S_z range, suggesting that it requires a delicate balance of certain parameters, among which the radiation field. The observations during the burst tails suggest that the NBO mechanism does not switch on instantly but rather becomes stronger in a more gradual way. Spectral fits during the bursts (Kuulkers 2001) suggest that the spectral properties of the accretion flow itself are not affected much by the increase in radiation.

Like the HBO, the NBO/FBO in GX 17+2 was discovered with *EXOSAT* (Stella et al. 1985, 1987). Kuulkers et al. (1997) found the NBO between $S_z=1.4$ and $S_z=2.0$, although it only had Q values higher than 1.5 above $S_z=1.6$. The frequencies were somewhat higher (~ 0.5 Hz) than we found, but this can be explained by the fact that the LFN was not fitted separately, but with the same Lorentzian that was used for NBO. The frequencies of the LFN that we found in the same S_z range are ~ 10 Hz, so if the LFN is not fitted, the fitted frequency for the NBO is higher than its true frequency. This effect is rather small in our data selections (~ 0.2 Hz), but will be probably high enough for the lower quality *EXOSAT* data to explain the frequency difference. The rms amplitudes of the NBO were lower than those we found, even though we fitted the LFN separately. This is due to the higher energy band that we used; the NBO in GX 17+2 and other Z sources becomes stronger towards higher energies (see Homan et al., in preparation, van der Klis 1995a). The FBO was only detected once in the *EXOSAT* data, around $S_z=2.36$ and with a frequency of 16.1 Hz, which is a bit lower than we found at a similar S_z , possibly because the LFN was not fitted separately (see above). In the *Ginga* data (Penninx et al. 1990) the FBO was found over a larger frequency range: 12.6-18.6 Hz, where we only take into account QPOs with $Q>1.5$. The frequency of the FBO clearly increased with the position on the FB. The NBO was found between 5.5 Hz and 7.7 Hz, with no clear dependence on the position on the NB. There was

one observation of a QPO with an intermediate frequency of 9.4 Hz, but it was found on the FB far from the NB/FB vertex and is probably similar to the LFN we found on the FB. Note that both in the *EXOSAT* and *Ginga* data peaks were found, in a similar frequency range as the NBO and FBO, but with much larger widths. These peaks were likely blends of the NBO/FBO with LFN, or only LFN.

In our data set we found the NBO between $S_z=1.6$ and $S_z=2.1$, although it may already have been present as a very broad feature as early as $S_z=1.4$. Its frequency, which was on average ~ 6.8 Hz, did not change by more than ~ 0.5 Hz in this interval. Between $S_z=2.0$ and $S_z=2.1$, the NBO (6.86 ± 0.10 Hz) was detected simultaneously with the FBO ($13.9^{+0.6}_{-0.4}$ Hz). Above $S_z=2.1$ the FBO frequency increased, to ~ 23 Hz at $S_z=2.65$. Note that the simultaneous presence of the NBO and FBO between $S_z=2.0$ and $S_z=2.1$ is likely an artifact of the S_z selection method. Inspection of dynamical power spectra showed that they were never present at the same time. It is interesting though, that in that S_z selection their frequencies differed by a factor that is consistent with a factor 2, which is suggestive of mode switching of the NBO/FBO. However, there is evidence for QPOs with intermediate frequencies, which undermines that idea. So, two major changes occurred at the NB/FB vertex: first, the frequency changed from being more or less constant to being strongly correlated with S_z . Second, the frequency increased by a factor consistent with 2. The first effect was also clearly observed in Sco X-1 by Dieters & van der Klis (2000). Although a sharp increase occurred in the NBO/FBO frequency around $S_z=2.0$ in Sco X-1, the transition contained more intermediate frequencies. However, like in GX 17+2 it was not resolved and it is therefore still possible that frequency switching of some kind occurred. The only way to see whether the frequencies really gradually transform into each other is to study the power spectral changes as a function of time. However, the quality of the GX 17+2 data is not sufficient to perform such a study.

For two Z sources, GX 340+0 (Jonker et al. 2000b) and Sco X-1 (Priedhorsky et al. 1986), asymmetries of the NBO peaks have been reported. We suggest that in both sources the component responsible for the asymmetry is the LFN, which between $S_z=1.6$ and $S_z=2.1$ was found at the high frequency side of the NBO. On the other hand, as was already mentioned by Jonker et al. (2000b), high frequency shoulders are also observed for HBOs and for low frequency QPOs in black holes. It might be that these shoulders are related to the QPO mechanisms and were accidentally fit by the LFN, and interpreted as such, in our case.

The presence of the NBO/FBO in the Z sources has often been related to the fact that these sources accrete at near Eddington mass accretion rates. It is thought that at these high mass accretion rates a significant fraction of the accretion flow is in the form of a thick and perhaps spherical flow. Also, the effects of radiation pressure are thought to play an important role in this regime. The model for the NBO by Fortner et al. (1989) is based on a radiation feedback mechanism in a spherical accretion flow. Their simulations revealed the presence of ~ 6 Hz oscillations in the optical depth of the spherical accretion flow. They suggest that the mechanism may excite photo-hydrodynamic modes with similar frequencies. Near and above the Eddington luminosity these modes cause a segregation of the accreting gas and outgoing radiation, allowing accretion to continue at these luminosities. As a result the effective gravity

increases with luminosity, thereby increasing the frequency of these modes. This could explain the steep frequency increase of the FBO above $S_z=2.0$. Another model for the NBO was proposed by Alpar et al. (1992), in which the NBO frequency is basically that of sound waves in a thickened accretion disk. This model does not explain how the NBO changes into the FBO. A major problem for both models could be the recently discovered NBO/FBO-like QPOs in the two atoll sources 4U 1820–30 (Wijnands et al. 1999) and XTE J1806–246 (Wijnands & van der Klis 1999b). Certainly in the first source the luminosity is believed to be only $\sim 20\text{--}40\%$ of the Eddington luminosity, while near-Eddington luminosities are required in both models.

4.1.5. Noise Components - LFN, VLFN

The main difference between the *RXTE* and *EXOSAT* power spectra is the lack of HFN in the former. In the *EXOSAT* data HFN was found on all branches, up to frequencies of ~ 150 Hz. However, no HFN was found in our data set, which either means that the presence of HFN in GX 17+2 is subject to long term changes or that the HFN in *EXOSAT* was (partly) due to instrumental effects. A study of *EXOSAT* data of several sources (including background-only observations) by Berger & van der Klis (1994) showed that a component with an rms amplitude of $\sim 3\%$ is always present in the frequency range where the HFN was often found by Kuulkers et al. (1997) (~ 100 Hz, see also Berger & van der Klis 1998), suggesting the latter to be true. However, HFN was sometimes ($S_z=0.0\text{--}1.0$) also present at lower frequencies (20–50 Hz) with strengths too high to be explained by instrumental effects (4–5% rms). It might be that in those cases the same component was fitted that we call the sub-harmonic of the HBO. This component extended up to the same frequencies. The similar rms amplitudes and their dependence on S_z that we found seem to confirm this idea.

Like in the *Ginga* and *EXOSAT* data the VLFN was found on all branches. The rms amplitudes of the VLFN in our data seem to be lower than in the *EXOSAT* data as reported by Kuulkers et al. (1997). However, we only measured the strength of the VLFN between 0.1 and 1 Hz, whereas they extrapolated down to 0.01 Hz. We obtain similar rms amplitudes when we apply the same extrapolation. Because the VLFN is steeper on the FB, the effects of this extrapolation are more pronounced on that branch than on the HB and NB. On the FB the rms amplitude increases from $\sim 1\%$ to more than 3%, on the other branches the increases are in the order of $\sim 0.2\%$ rms. The power law indices are consistent with those found by Kuulkers et al. (1997). Past measurements of the energy spectrum of the VLFN suggest that it is caused by motion of the source along the Z (van der Klis 1986, 1991; Lewin et al. 1992). The strength of the VLFN (Fig. 11) and the speed along the Z track ($\langle V_z \rangle$, see Figure 4) should therefore have a similar dependence on S_z . Our results are inconclusive; although some correlations are observed (the increase above $S_z=3$, and the steep increase around $S_z=2$) there are also some differences. Most notable is the dip in the VLFN strength around $S_z=3$, which is not observed as a decrease in $\langle V_z \rangle$. It is possible that due to the steepness of the VLFN around $S_z=2.5$ most of its power was outside the range in which we determined the strength.

The LFN was not fitted as a separate component by Penninx et al. (1990). Kuulkers et al. (1997) reported LFN between $S_z=-0.8$ and $S_z=1.2$. Our data show much clearer relations of the LFN parameters with S_z than the *EXOSAT* data, at least in the S_z range where it was found by Kuulkers et al.

(1997). However, due to the large error bars in Kuulkers et al. (1997) the results are consistent with each other. In our data, the LFN followed the behavior of the HBO, both in strength and frequency, until the latter disappeared ($< S_z = 2.1$). Between $S_z=2.1$ and $S_z=2.8$ the behavior is rather complex and probably considerably influenced by the presence of the NBO/FBO. Above $S_z=3.0$ the behavior was rather clean, with a decrease in strength and an increase in frequency. It is not clear, however, whether the LFN on the FB is the same as that on the HB and NB. Unfortunately no HBO was observed above $S_z=2.1$ to compare its behavior with. Van der Klis et al. (1997) suggested that in Sco X-1 the NBO/FBO emerged from the LFN. This seems not to be the case in GX 17+2, since the rms amplitude of the LFN already starts to decrease well before the NBO appears. Moreover, ν_{max} shows a gradual increase between $S_z=-0.6$ and $S_z=1.4$ to values well above the NBO frequency. A comparative study by Wijnands & van der Klis (1999a) strongly suggests that LFN has a similar origin as the band-limited noise component in atoll sources, BHCs, and the millisecond X-ray pulsar SAX 1808.4-3658. They suggest that this noise component is produced in the accretion disk, and does not require the presence of magnetosphere or solid surface.

4.2. Spectral Behavior

In our observations GX 17+2 traced out the well known Z-like tracks in the CD and HID. In addition to motion along this track, we also observed secular motion of the Z track itself in the HID of epoch 3 (see Figure 2), as was already reported by Wijnands et al. (1997a) (see also Kuulkers et al. 1997, for a possible shift in the *EXOSAT* HID of GX 17+2).

It is commonly believed that the motion of the source along and its position on the Z track are determined by the mass accretion rate (\dot{M}) through the inner accretion disk and onto the neutron star, increasing from the HB to the FB. Even though the count rates actually decrease on the NB and in some sources also on the FB (implying an anti-correlation between \dot{M} and flux) there are several observational results that support this view: (1) the frequencies of the HBO and kHz QPOs, that in many models are directly related to \dot{M} , gradually increase from HB to NB (and in Sco X-1 even to the FB, see van der Klis et al. 1996). (2) The optical and UV flux increase from HB to FB (Hasinger et al. 1990; Vrtilek et al. 1990; van Paradijs et al. 1990; Vrtilek et al. 1991; Hertz et al. 1992; Augusteijn et al. 1992); in X-ray binaries they are thought to be due to reprocessing of X-rays from the central source in the outer accretion disk. There are several reasons to believe that the optical and UV flux are better tracers of the mass accretion rate than the X-ray flux (Hasinger et al. 1990). This would then solve the apparent anti-correlation between \dot{M} and the (X-ray) flux (Hasinger et al. 1990). (3) Motion of a source is always along the Z track; jumps between branches are never observed, in accordance with the assumption that \dot{M} varies continuously.

It has been found that secular motion of the Z tracks in the CDs of the Cyg-like sources does not affect the relation between the rapid variability properties and source position along the track (see, e.g. Kuulkers et al. 1994; Jonker et al. 2000b, however see Wijnands & van der Klis 2001). In view of the \dot{M} -dominated picture mentioned above, these changes can therefore not be due to changes in \dot{M} , but should have a different origin. It has been suggested that the Cyg-like sources are viewed at a higher inclination than the Sco-like sources (Kuulkers et al. 1994). The differences in shapes of the Z tracks and some of

the variability properties are also explained in this model (Kuulkers et al. 1994; Kuulkers & van der Klis 1995). Psaltis et al. (1995) suggest that the difference among the Z sources might be explained by a difference in the magnetic field strength, with the Sco-like sources having a lower magnetic field.

In the last few years results have been obtained that may challenge the \dot{M} -dominated picture. These results are mainly due to the arrival of *RXTE*, whose high quality data revealed new phenomena and allowed for a better comparison between different classes of X-ray binaries. In the following we discuss how some of our results of GX 17+2 conflict with the \dot{M} -dominated picture.

The frequency of the HBO in GX17+2 starts to decrease when the source is half way the NB. Although there are several explanations for this (see Section 4.1.1), it means that the first assumption given above (i.e. QPO frequencies increase with \dot{M}) is not as solid as it seemed a few years ago.

The theory of type I X-ray bursts predicts that their properties change and correlate with \dot{M} (Fujimoto et al. 1981; Fushiki & Lamb 1987). A study of the type I X-ray bursts in GX 17+2 by Kuulkers (2001) showed that their properties did not correlate well with the position along the Z track at which they occurred, and therefore not well with the inferred \dot{M} . Although other explanations are possible (see Kuulkers 2001), this could mean that \dot{M} does not determine the position of the source along the Z track. However, note that there does seem to be a correlation between the probability that a burst occurs and position along the Z track, which is not easy to explain other than by a variation of \dot{M} (onto the neutron star) along the Z track.

Recently, di Salvo et al. (2000) reported the discovery with BeppoSAX of a hard tail in the energy spectrum of GX 17+2. It increased in strength from the HB/NB vertex (where only upper limits on its strength could be determined) onto the HB. They also showed that the total 0.1–200 keV flux increased monotonically from the NB/FB vertex ($F_X = 1.52 \times 10^{-8} \text{ erg s}^{-1}$) to the top of the HB ($F_X = 1.84 \times 10^{-8} \text{ erg s}^{-1}$). This is different from the behavior of the 2.9–20.1 keV count rate (see Figure 3a), which increased from NB/FB vertex to the HB/NB vertex, but decreases afterwards. As can be seen from Figure 3b the behavior of the hard count rate confirms the findings of di Salvo et al. (2000). Also, there is no evidence for a change in its behavior near the HB/NB vertex. Unfortunately no BeppoSAX data were taken on the FB.

The behavior of the 0.1–200 keV flux on the NB and HB suggest that \dot{M} increases in the opposite direction from what is commonly assumed. However, since the flux changes are rather moderate ($\sim 20\%$), another option is that \dot{M} does not change at all along the Z track. In that case motion along the Z track (i.e. spectral change) is caused by another parameter, such as the inner disk radius, while \dot{M} remains constant (van der Klis 2000). A similar possibility was suggested by Homan et al. (2001) to explain the observed behavior of the black hole transient XTE J1550–564. They found that similar spectral changes occurred at different levels of the inferred mass accretion rate. The spectral changes were ascribed to an unknown parameter, which they suggested to be the inner disk radius (based on variability), the size of the Comptonizing region (based on spectral hardness), and/or the accretion flow geometry (based on radio brightness). If this also applies to the Z sources, the secular motion that is observed could perhaps be explained by changes in the \dot{M} . The apparent lack of a correlation between the type I burst properties and the position along the Z track could also be

explained, since \dot{M} would determine the properties of the bursts but no longer the spectral properties.

It is interesting to see that GX 17+2 and the Z sources, show in fact several similarities with XTE J1550–564 and other black hole sources. The first was already briefly mentioned above, and concerns the independent behavior of the hard and soft spectral components on the HB. This independence of the hard and soft spectral components is commonly observed in black hole candidates (BHCs, see Tanaka & Lewin 1995). There are several properties that correlate well with the spectral hardness in BHCs and also with the spectral hardness in Z sources, which increases from the NB to the HB (for the moment we will exclude the FB from the comparison; it will be discussed later). These properties are the radio flux, the optical flux, and to a certain degree also QPO frequencies. (1) The radio flux in BHCs is correlated with the spectral hardness (Fender et al. 1999; Fender 2001, and references therein). This is also true for GX 17+2, where the radio flux increases from the NB to the HB (Penninx et al. 1988). Sco X-1 (Hjellming et al. 1990b) and Cyg X-2 (Hjellming et al. 1990a) show similar behavior, whereas GX 5-1 only showed one radio flare on the NB (Tan et al. 1992); the behavior of GX 349+2 (Cooke & Ponman 1991) and GX 340+0 (Penninx et al. 1993) has not been studied in that much detail. The behavior of the radio flux suggests that as the spectral hardness increases, part of the flow onto the neutron star evolves into an outflow. (2) Jain et al. (2001) found that in XTE J1550–564 the optical flux decreased during several small X-ray flares in which the hard spectral component became stronger. Although the optical counterpart of GX 17+2 (Callanan et al. 1999; Deutscher et al. 1999) has never been studied in much detail, this behavior is similar to the anti-correlation between the hard color and optical/UV flux on the NB and HB in the Z sources Cyg X-2 (Hasinger et al. 1990; Vrtilek et al. 1990; van Paradijs et al. 1990) and Sco X-1 (Vrtilek et al. 1991; Hertz et al. 1992; Augusteijn et al. 1992). (3) In XTE J1550–564 the frequencies of the low and high frequency QPO anti-correlate with the strength of the hard spectral component (Homan et al. 2001). This is also found in GX 17+2 for the kHz QPOs and HBO (compare Figure 3b with Figures 6 and 12) and other Z sources. The only exception is the correlation between the HBO frequency and spectral hardness that we observed on the lower NB. In that respect it is interesting to mention that Rutledge et al. (1999) report a switch from a correlation to an anti-correlation between the QPO frequency and spectral hardness in several BHCs, when the latter increases beyond a certain value. In addition to the QPO frequencies also the band-limited noise behaves similarly. It increases with spectral hardness, both in BHCs and Z sources (van der Klis 1995a)

It is tempting to compare the different black hole states (Tanaka & Lewin 1995; van der Klis 1995a) with those of the Z sources. Based on the above similarities, we suggest that the HB corresponds to the low state, the NB to the intermediate and/or very high state state, and the FB to the high state. However, there are still considerable differences: the low state spectra are much harder than those of the HB, and the noise in the low state is also much stronger. Also flaring is not observed in the black hole high state. However, in both the high state and FB the variability at high frequencies (> 50 Hz) is extremely weak. It is not clear if and how the presence of a solid surface can explain these differences.

Our analysis has revealed several new properties of the low and high frequency QPOs in GX 17+2, which are of general interest to the understanding of these phenomena in neutron star LMXBs. The most important findings are the variable frequency difference of the kHz QPO, the non-monotonic relation between the HBO and the upper kHz QPO, the similar Q values of the HBO, its second harmonic, and the kHz QPOs and the suppression of the NBO amplitude during type I X-ray bursts. These new findings can in principle be used to put constraints on, or even rule out, some of the models that have been proposed for these low and high frequency QPOs in neutron star LMXBs. In the following we summarize what the implications of each of our new findings are for some of the proposed models. Note that, as is often indicated by the various authors themselves, many of the models discussed below are oversimplifications. Also, most of the models do not explicitly predict the behavior we observed and from the available literature it is not always clear whether or not a certain model can account for the observed behavior. Nonetheless, we feel that it is interesting to explicitly test some of the basic (physical) assumptions of the various models. The models we consider are the relativistic precession model (RPM, Stella & Vietri 1998, 1999; Stella et al. 1999) and the sonic point beat frequency model (SPBFM, Miller et al. 1998; Lamb & Miller 2001), which have already been discussed extensively in Section 4.1, the 'disk-filter' model (DFM) by Psaltis & Norman (2001), which produces the same frequencies as the RPM, but with minor corrections, the trapped disk mode model (TDMM, see Wagoner 1999, and references therein), and the two oscillator model (TOM, Titarchuk & Osherovich 1999; Osherovich & Titarchuk 1999). Note that the TDMM was developed for the high frequency QPOs in black hole LMXBs, but that it may also be applicable to neutron star LMXBs.

- HBO-kHz QPO frequencies: The RPM can explain a turnover of the HBO-kHz QPO frequency relation; in this model it can be due to the growing importance of classical precession at smaller orbital radii. Assuming that the observed HBO is four times the predicted frequency, our results imply rather extreme neutron star parameters: a high neutron star spin frequency (~ 500 – 700 Hz), a neutron star mass of more than $2 M_{\odot}$, and a hard equation of state. The same may hold for the DFM. The SPBFM also has some difficulties with the observed relation; it requires a decoupling of part of the accretion flow from the disk flow outside the magnetosphere (to explain the HBO frequency decrease) and subsequently that this flow recouples with the disk flow before the sonic point radius is reached (to explain the increase in the kHz QPO frequencies). Judging from figures in Wagoner (1999) and Titarchuk, Osherovich, & Kuznetsov (1999) both the TDMM and TOM can in principle also account for a turnover in the relation between the low frequency (HBO) and high frequency (kHz QPO) peaks, although it is not clear how this turnover can be used to constrain physical parameters.
- Variable kHz QPO separation: Although not significant at a 3 sigma level, the kHz QPO separation seems to

decrease both towards low and high values for the upper kHz QPO frequency. The RPM basically predicts such behavior, but not in the way as we observed it, as apparent from Figure 13. We assume that the DFM has the same difficulties with the observed behavior as the RPM. The SPBFM apparently can not explain the possible decrease of the frequency separation at the low frequency side (Section 3.3); it is not clear to us whether the TOM can explain this. Both models can account for the decrease towards high frequencies. The TDMM does not explicitly deal with twin high frequency QPOs, and therefore not with their frequency separation either.

- Similar Q values: In the SPBFM the low and high frequency QPOs are produced independently from each other and there is no a priori reason why their Q values should be similar. In the RPM, all the oscillations are produced by a single test particle. Lifetime broadening and the presence of multiple test particles both lead to different Q values for the low and high frequency QPO. Frequency modulation could work for both models, but only if the modulating parameter is not the same as the one that causes the motion along the Z track. It is not clear to us what the predicted behavior of the Q values is in the DFM, TDMM, and TOM.

From the above points it is clear that none of the current models can satisfactorily explain all the observed phenomena, either because the models predict something else, or they do not deal with the specific subject at all.

The observed behavior of the NBO during two type I X-ray bursts showed that this QPO is very sensitive to the strength of the radiation field from the neutron star. This seems to confirm the basic idea behind the feedback mechanism model that was proposed by Fortner et al. (1989), i.e. it requires a delicate balance between the inwards directed forces and the radiation field.

Finally, we compared the behavior of GX 17+2 (and the other Z sources) with that of (some) black hole LMXBs. Many similarities exist, particularly with regard to the relation between the hard spectral component on the one hand, and variability properties (QPO frequency, broad band noise strength) and radio flux on the other. Based on recent findings in black hole LMXBs we consider the possibility that the mass accretion might not be the parameter that determines the position along the Z track after all.

This work was supported in part by the Netherlands Organization for Scientific Research (NWO) grant 614-51-002 and by NWO Spinoza grant 08-0 to E.P.J. van den Heuvel. RW was supported by NASA through the Chandra Postdoctoral Fellowship grant number PF9-10010 awarded by the Chandra X-ray Center, which is operated by the Smithsonian Astrophysical Observatory for NASA under contract NAS8-39073. MM is a fellow of the Consejo Nacional de Investigaciones Científicas y Técnicas de la República Argentina. WHGL is grateful for support from NASA.

REFERENCES

Alpar, M. A., Hasinger, G., Shaham, J., & Yancopoulos, S. 1992, *A&A*, 257, 627

Alpar, M. A. & Shaham, J. 1985, *Nature*, 316, 239

Augusteijn, T., Karatasos, K., Papadakis, M., et al. 1992, *A&A*, 265, 177

Belloni, T., van der Klis, M., Lewin, W. H. G., et al. 1997, *A&A*, 322, 857

Berger, M. & van der Klis, M. 1994, *A&A*, 292, 175

—. 1998, *A&A*, 340, 143

Bradt, H. V., Rothschild, R. E., & Swank, J. H. 1993, *A&AS*, 97, 355

Callanan, P. J., Filippenko, A. V., & Garcia, M. R. 1999, *IAU Circ.*, 7219

Campana, S. 2000, *ApJ*, 534, L79

Cooke, B. A. & Ponman, T. J. 1991, *A&A*, 244, 358

Cui, W. 2000, *ApJ*, 534, L31

Deutsch, E. W., Margon, B., Anderson, S. F., Wachter, S., & Goss, W. M. 1999, *ApJ*, 524, 406

di Salvo, T., Méndez, M., van der Klis, M., Ford, E., & Robba, N. R. 2001, *ApJ* di Salvo, T., Stella, L., Robba, N. R., et al. 2000, *ApJ*, 544, L119

Dieters, S. W. & van der Klis, M. 2000, *MNRAS*, 311, 201

Fender, R. 2001, To be published in Proc. ESO workshop ‘Black Holes in binaries and galactic nuclei’, Eds. L. Kaper, E.P.J. van den Heuvel and P.A. Woudt, Springer-Verlag, astro-ph/9911176

Fender, R., Corbel, S., Tzioumis, T., et al. 1999, *ApJ*, 519, L165

Ford, E. C., van der Klis, M., & Kaaret, P. 1998a, *ApJ*, 498, L41

Ford, E. C., van der Klis, M., van Paradijs, J., et al. 1998b, *ApJ*, 508, L155

Fortner, B., Lamb, F. K., & Miller, G. S. 1989, *Nature*, 342, 775

Fujimoto, M. Y., Hanawa, T., & Miyaji, S. 1981, *ApJ*, 267

Fushiki, I. & Lamb, D. Q. 1987, *ApJ*, 323, L55

Hasinger, G. & van der Klis, M. 1989, *A&A*, 225, 79

Hasinger, G., van der Klis, M., Ebisawa, K., Dotani, T., & Mitsuda, K. 1990, *A&A*, 235, 131

Hertz, P., Vaughan, B., Wood, K. S., et al. 1992, *ApJ*, 396, 201

Hjellming, R. M., Han, X. H., Cordova, F. A., & Hasinger, G. 1990a, *A&A*, 235, 147

Hjellming, R. M., Stewart, R. T., White, G. L., et al. 1990b, *ApJ*, 365, 681

Homan, J., Jonker, P. G., Wijnands, R., van der Klis, M., & van Paradijs, J. 1999, *ApJ*, 516, L91

Homan, J., Wijnands, R., van der Klis, M., et al. 2001, *ApJS*, 132, in press

Jahoda, K., Swank, J. H., Giles, A. B., et al. 1996, *Proc. SPIE*, 2808, 59

Jain, R. J., Bailyn, C. D., Orosz, J. A., et al. 2001, *ApJ*, in press

Jonker, P. G., van der Klis, M., Homan, J., et al. 2000a, *ApJ*, 531, 453

Jonker, P. G., van der Klis, M., & Wijnands, R. 1999, *ApJ*, 511, L41

Jonker, P. G., van der Klis, M., Wijnands, R., et al. 2000b, *ApJ*, 537, 374

Jonker, P. G., Wijnands, R., van der Klis, M., et al. 1998, *ApJ*, 499, L191

Kuulkers, E. & van der Klis, M. 1995, *A&A*, 303, 801

—. 1996, *A&A*, 314, 567

Kuulkers, E., van der Klis, M., Oosterbroek, T., et al. 1994, *A&A*, 289, 795

Kuulkers, E., van der Klis, M., Oosterbroek, T., van Paradijs, J., & Lewin, W. H. G. 1997, *MNRAS*, 287, 495

Kuulkers, E., van der Klis, M., & van Paradijs, J. 1995, *ApJ*, 450, 748

Kuulkers, E., van der Klis, M., & Vaughan, B. A. 1996, *A&A*, 311, 197

Kuulkers, E. e. a. 2001, *A&A*, to be submitted

Lamb, F. K. & Miller, M. C. 2001, *ApJ*, in preparation, astro-ph/0007460

Lamb, F. K., Shibazaki, N., Alpar, M. A., & Shaham, J. 1985, *Nature*, 317, 681

Langmeier, A., Hasinger, G., & Truemper, J. 1990, *A&A*, 228, 89

Lewin, W. H. G., Lubin, L. M., Tan, J., et al. 1992, *MNRAS*, 256, 545

Markovic, D. & Lamb, F. K. 2001, *MNRAS*, submitted, astro-ph/0009169

Méndez, M. & van der Klis, M. 1999, *ApJ*, 517, L51

Méndez, M., van der Klis, M., van Paradijs, J., et al. 1998a, *ApJ*, 494, L65

Méndez, M., van der Klis, M., Wijnands, R., et al. 1998b, *ApJ*, 505, L23

Miller, M. C., Lamb, F. K., & Psaltis, D. 1998, *ApJ*, 508, 791

Morsink, S. M. & Stella, L. 1999, *ApJ*, 513, 827

Osherovich, V. & Titarchuk, L. 1999, *ApJ*, 522, L113

Penninx, W., Lewin, W. H. G., Mitsuda, K., et al. 1990, *MNRAS*, 243, 114

Penninx, W., Lewin, W. H. G., Zijlstra, A. A., Mitsuda, K., & van Paradijs, J. 1988, *Nature*, 336, 146

Penninx, W., Zwarthoed, G. A. A., van Paradijs, J., et al. 1993, *A&A*, 267, 92

Press, W. H., Teukolsky, S. A., Vetterling, W. T., & Flannery, B. P. 1992, *Numerical recipes in FORTRAN. The art of scientific computing* (Cambridge: University Press, [c]1992, 2nd ed.)

Priedhorsky, W., Hasinger, G., Lewin, W. H. G., et al. 1986, *ApJ*, 306, L91

Psaltis, D., Belloni, T., & van der Klis, M. 1999, *ApJ*, 520, 262

Psaltis, D., Lamb, F. K., & Miller, G. S. 1995, *ApJ*, 454, L137

Psaltis, D., Méndez, M., Wijnands, R., et al. 1998, *ApJ*, 501, L95

Psaltis, D. & Norman, C. 2001, *ApJ*, submitted

Rutledge, R. E., Lewin, W. H. G., van der Klis, M., et al. 1999, *ApJS*, 124, 265

Smale, A. P. 1998, *ApJ*, 498, 141

Stella, L., Parmar, A. N., & White, N. E. 1985, *IAU Circ.*, 4102

—. 1987, *ApJ*, 321, 418

Stella, L. & Vietri, M. 1998, *ApJ*, 492, L59

—. 1999, *Phys. Rev. Lett.*, 82, 17

Stella, L., Vietri, M., & Morsink, S. M. 1999, *ApJ*, 524, L63

Strohmayer, T. E., Zhang, W., Swank, J. H., et al. 1996, *ApJ*, 469, L9

Tan, J., Lewin, W. H. G., Hjellming, R. M., et al. 1992, *ApJ*, 385, 314

Tanaka, Y. & Lewin, W. H. G. 1995, in *X-ray binaries (Cambridge Astrophysics Series)*, Cambridge, MA: Cambridge University Press, [c]1995, edited by Lewin, Walter H.G.; Van Paradijs, Jan; Van den Heuvel, Edward P.J.), p. 126

Titarchuk, L. & Osherovich, V. 1999, *ApJ*, 518, L95

Titarchuk, L., Osherovich, V., & Kuznetsov, S. 1999, *ApJ*, 525, L129

van der Klis, M. 1986, in *LNP Vol. 266: The Physics of Accretion onto Compact Objects*, p. 157

van der Klis, M. 1989, in *Proceedings of the NATO Advanced Study Institute on Timing Neutron Stars*, held in Çeşme, Izmir, Turkey, April 4–15, 1988. Editors, H. Ögelman and E.P.J. van den Heuvel; Publisher, Kluwer Academic, Dordrecht, The Netherlands, Boston, Massachusetts, p. 27

van der Klis, M. 1991, in *NATO ASIC Proc. 344: Neutron Stars*, p. 319

van der Klis, M. 1995a, in *X-ray binaries (Cambridge Astrophysics Series)*, Cambridge, MA: Cambridge University Press, [c]1995, edited by Lewin, Walter H.G.; Van Paradijs, Jan; Van den Heuvel, Edward P.J.), p. 252

van der Klis, M. 1995b, in *Proceedings of the NATO Advanced Study Institute on the Lives of the Neutron Stars*, held in Kemer, Turkey, August 29–September 12, 1993. Editor(s), M.A. Alpar, U. Kiziloglu, J. van Paradijs; Publisher, Kluwer Academic, Dordrecht, The Netherlands, Boston, Massachusetts, 1995., p. 301

—. 2000, *ARA&A*, 38, 717

van der Klis, M., Homan, J., Wijnands, R., et al. 1997a, *IAU Circ.*, 6565

van der Klis, M., Jansen, F., van Paradijs, J., et al. 1985, *Nature*, 316, 225

van der Klis, M., Swank, J. H., Zhang, W., et al. 1996, *ApJ*, 469, L1

van der Klis, M., Wijnands, R. A. D., Horne, K., & Chen, W. 1997b, *ApJ*, 481, L97

van Paradijs, J., Allington-Smith, J., Callanan, P., et al. 1990, *A&A*, 235, 156

van Straaten, S., Ford, E. C., van der Klis, M., Méndez, M., & Kaaret, P. 2000, *ApJ*, 540, 1049

Vrtilek, S. D., Penninx, W., Raymond, J. C., et al. 1991, *ApJ*, 376, 278

Vrtilek, S. D., Raymond, J. C., Garcia, M. R., et al. 1990, *A&A*, 235, 162

Wagoner, R. W. 1999, *Phys. Rep.*, 311, 259

Wijnands, R., Homan, J., van der Klis, M., et al. 1998a, *ApJ*, 493, L87

—. 1997a, *ApJ*, 490, L157

Wijnands, R., Méndez, M., van der Klis, M., et al. 1998b, *ApJ*, 504, L35

Wijnands, R. & van der Klis, M. 1999a, *ApJ*, 514, 939

—. 1999b, *ApJ*, 522, 965

—. 2001, *MNRAS*, in press

Wijnands, R., van der Klis, M., Kuulkers, E., Asai, K., & Hasinger, G. 1997b, *A&A*, 323, 399

Wijnands, R., van der Klis, M., Méndez, M., et al. 1998c, *ApJ*, 495, L39

Wijnands, R., van der Klis, M., Psaltis, D., et al. 1996, *ApJ*, 469, L5

Wijnands, R., van der Klis, M., & Rijkhorst, E. 1999, *ApJ*, 512, L39

Yu, W., van der Klis, M., & Jonker, P. 2001, *ApJ*, in prep.

Zhang, W. 1995, *XTE/PCA Internal Memo*

Zhang, W., Jahoda, K., Swank, J. H., Morgan, E. H., & Giles, A. B. 1995, *ApJ*, 449, 930

Zhang, W., Strohmayer, T. E., & Swank, J. H. 1998, *ApJ*, 500, L167

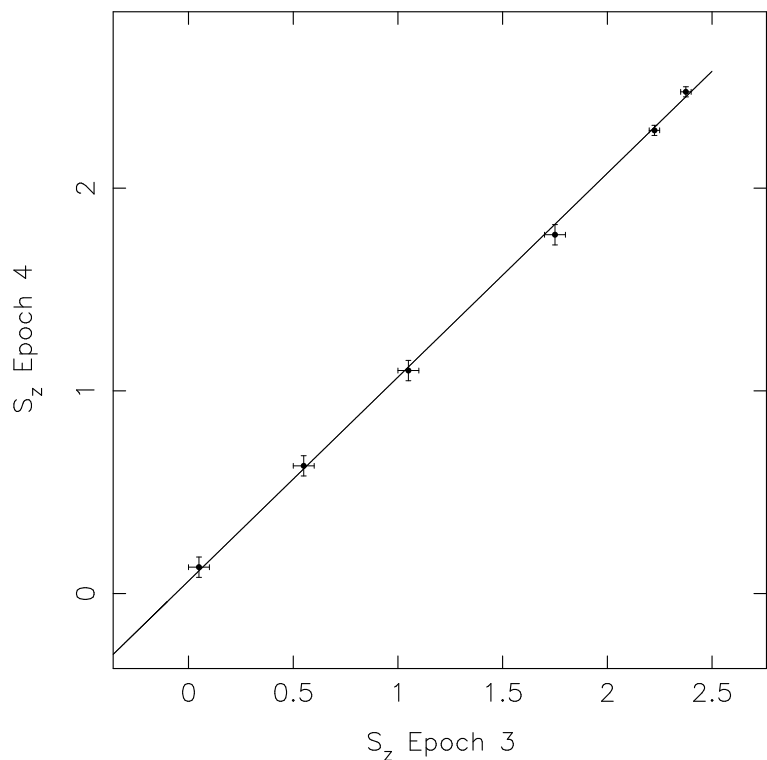


FIG. 1.— S_z selections with similar HBO or NBO/FBO frequencies for epoch 3 and epoch 4. The best linear relation between the two scales is $S_{z,epoch4} = (0.06 \pm 0.04) + (1.005 \pm 0.018)S_{z,epoch3}$. The errors are the widths of the S_z selections.

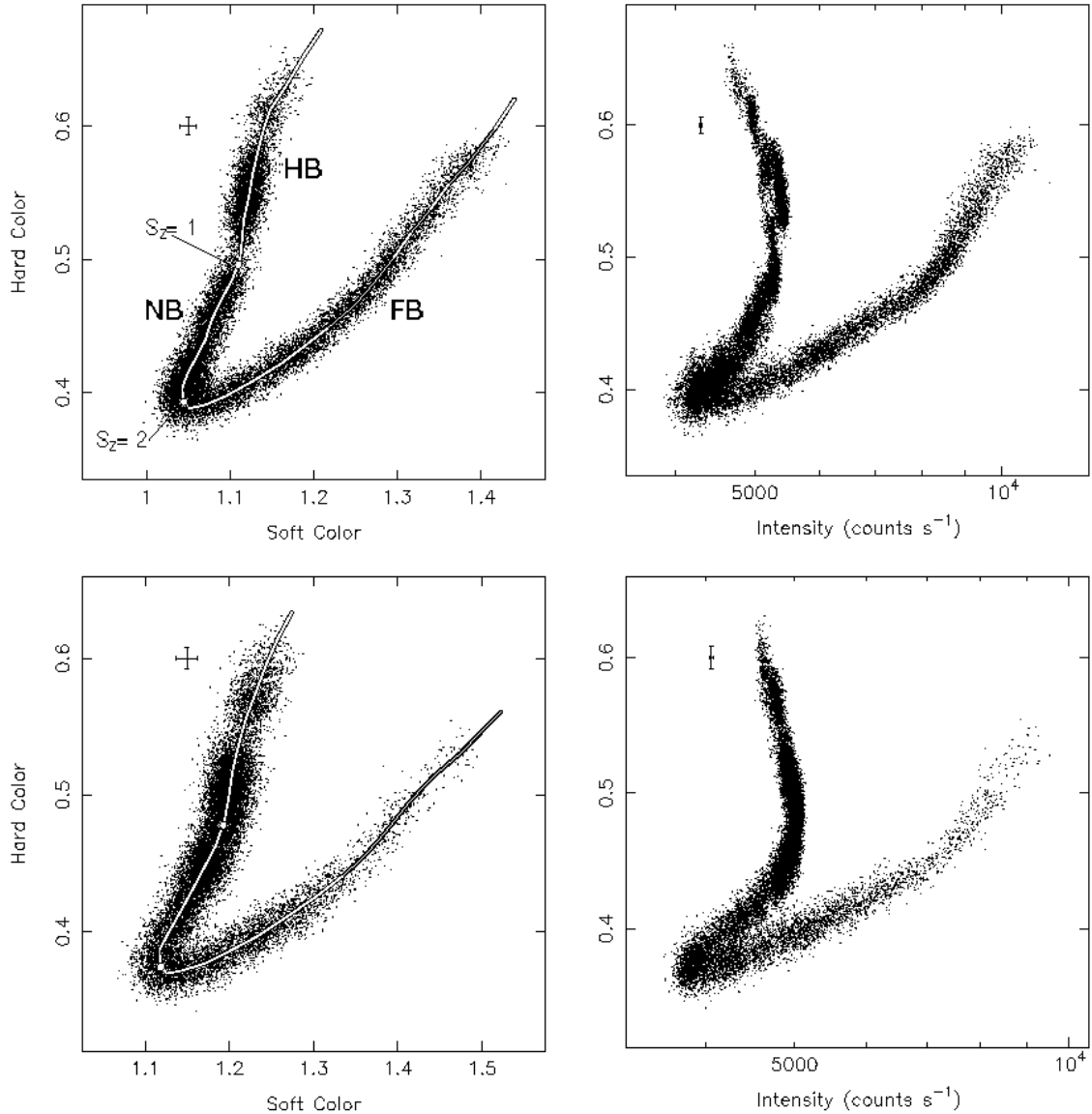


FIG. 2.— Color-color diagrams (left column) and Hardness-Intensity diagrams (right column) for the epoch 3 (top) and epoch 4 data (bottom). Each point represent a 16 s average. The splines and vertices (white circles) that were used for the S_z parameterization are shown, as are the typical error bars. See Table 3 for the energy bands used for the soft and hard color and intensity.

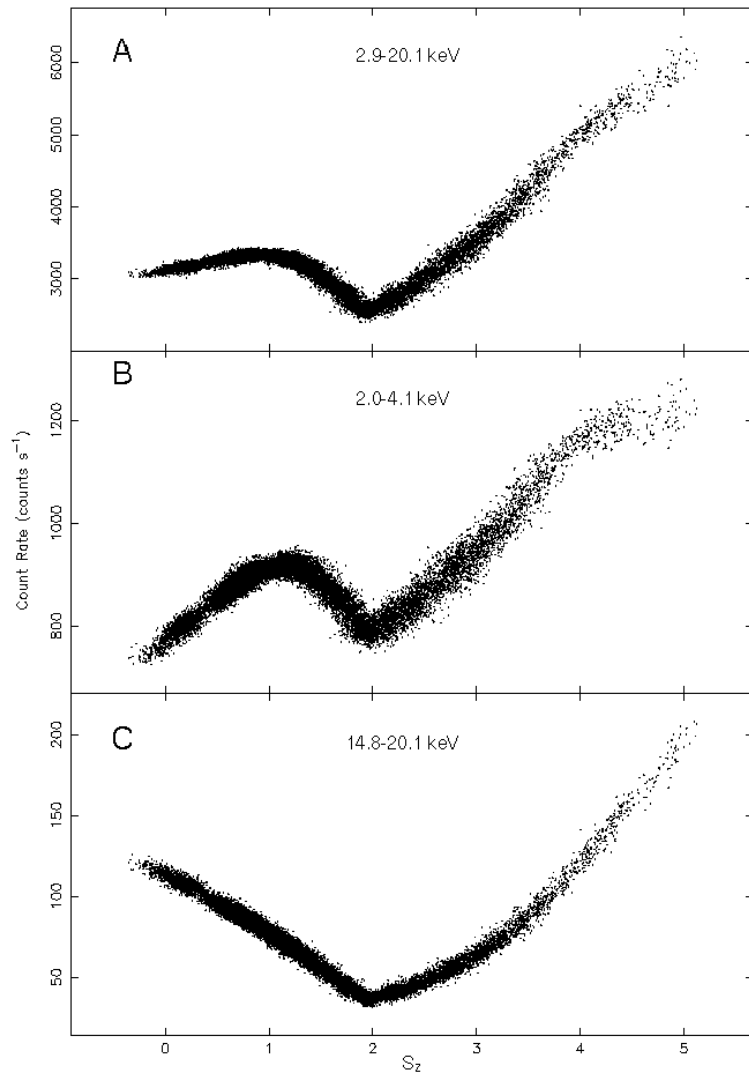


FIG. 3.— The count rate in three energy bands as a function of S_z (epoch 4 data only). The HB/NB vertex in the 2.9–20.1 keV band (a) is caused by the contribution from the low energies (b). This vertex does not show up at high energies (c).

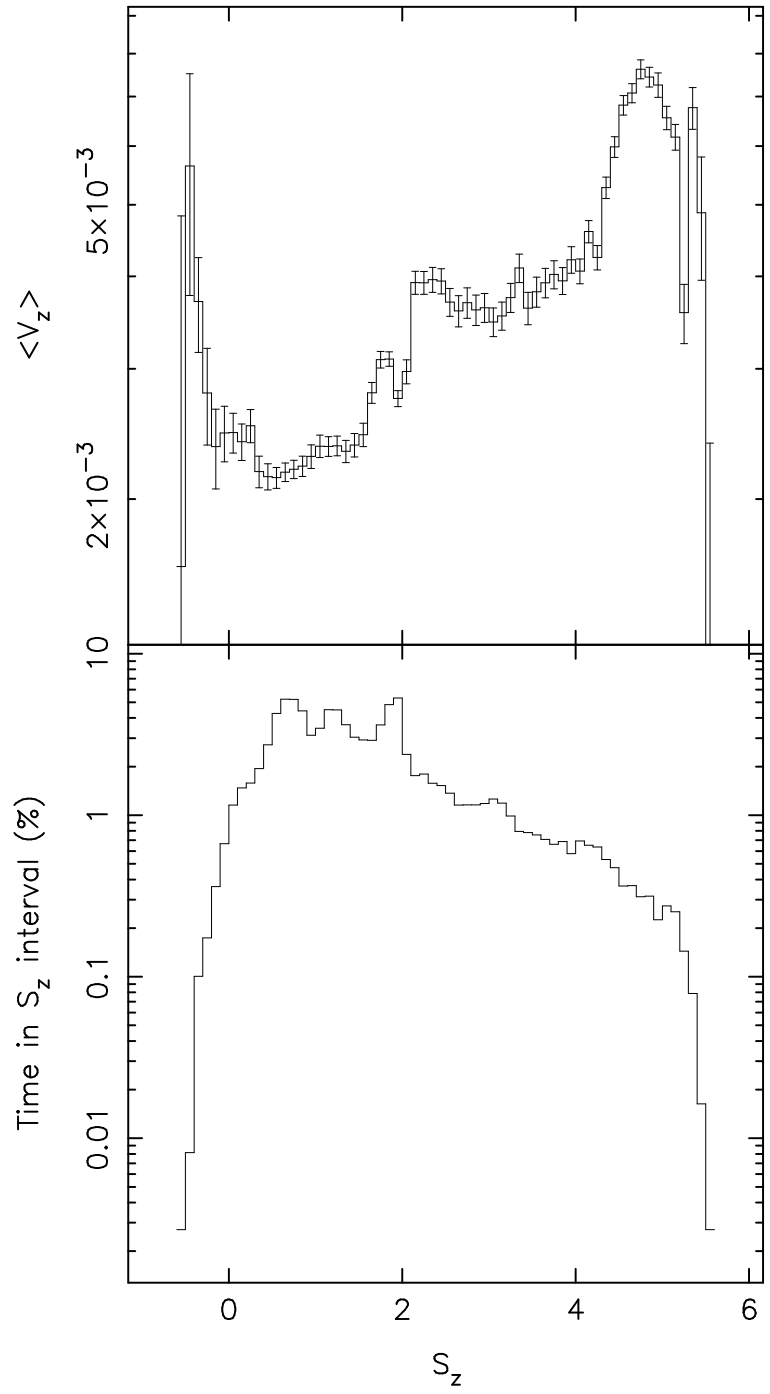


FIG. 4.— *Top:* The average speed along the Z track ($\langle V_z \rangle$). *Bottom:* the percentage of the time spent in each S_z -interval as a function of S_z .

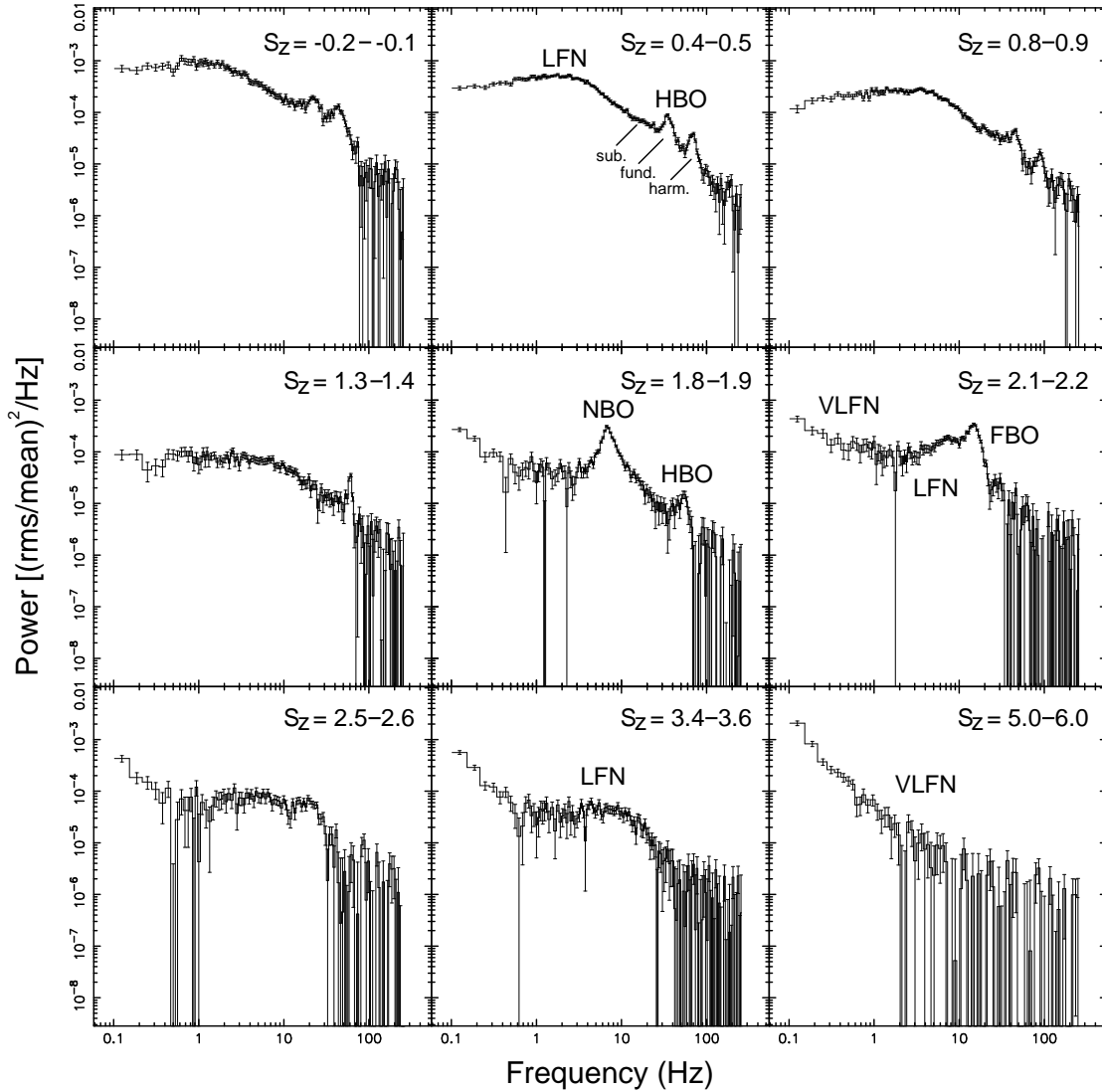


FIG. 5.— Power spectra (0.0625–256 Hz) for nine different S_z selections. The Poisson level was subtracted for all power spectra. The most important power spectral features are indicated.

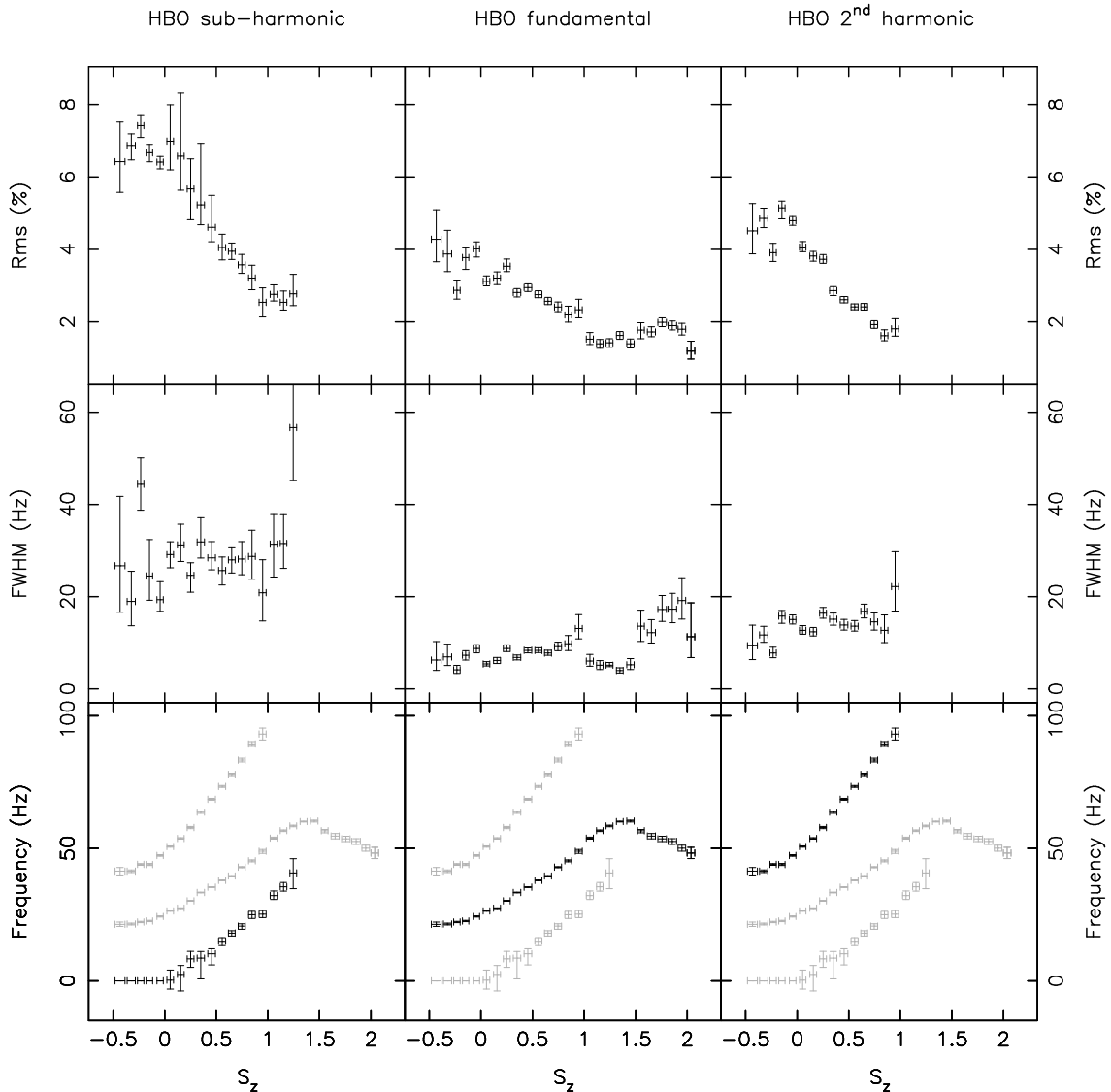


FIG. 6.—Properties of the HBO (middle column), its second harmonic (right column), and sub-harmonic (left column) as a function of S_z . For reasons of comparison the frequency of the other two QPOs (gray) are also plotted in the frequency plot of each QPO.

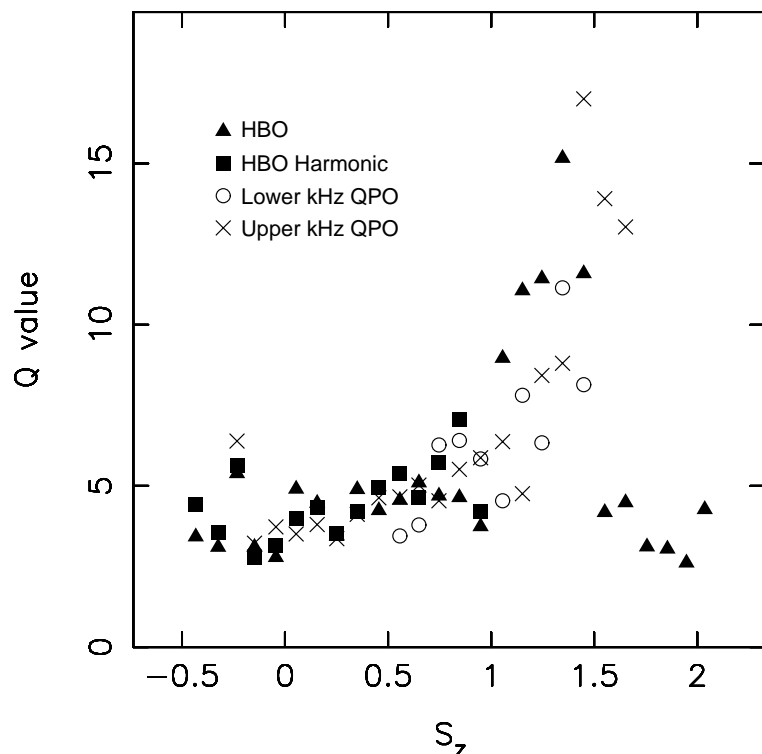


FIG. 7.—Q values (Frequency/FWHM) of the HBO, its harmonic, and the two kHz QPOs as a function of S_z . For reasons of clarity the error bars, which at a given S_z in general overlapped, were omitted.

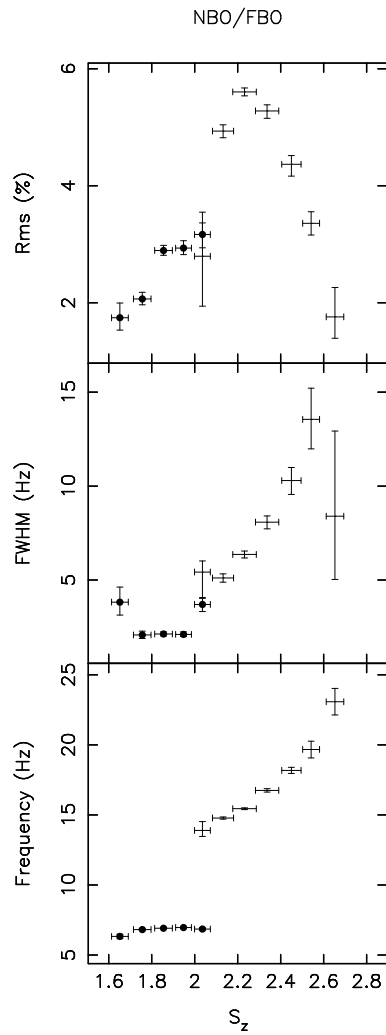


FIG. 8.—Properties of the NBO (filled circles) and FBO as a function S_z .

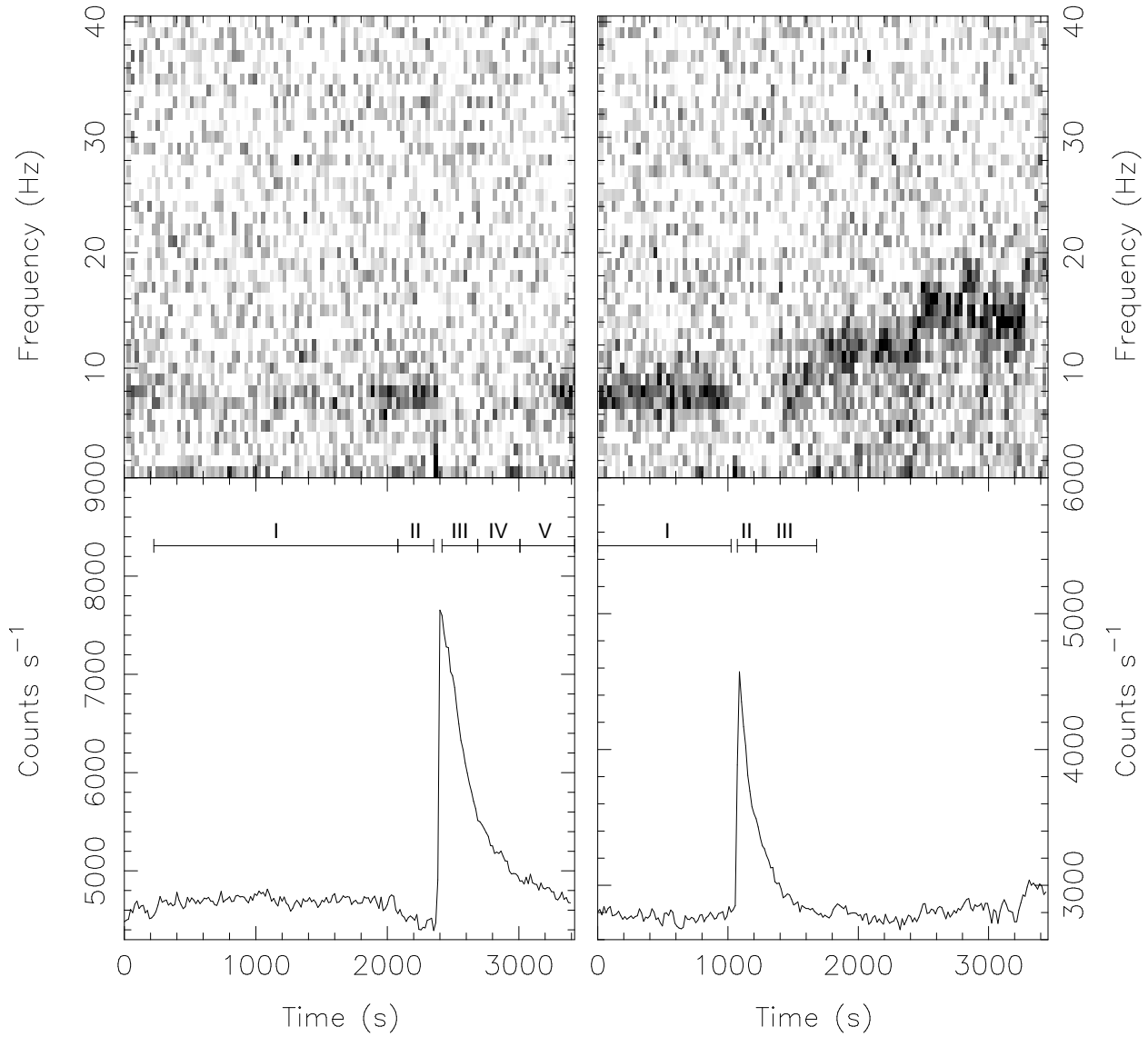


FIG. 9.— The dynamical power spectra (*top panels*) and light curves in the 2–60 keV band (*bottom panels*) of the two type I X-ray bursts in which we studied the behavior of the NBO/FBO (The November 1998 burst is shown on the left [5 PCUs] and the October 1999, burst on the right [3 PCUs].). The intervals in which we measured the NBO/FBO are indicated by Roman numerals (see Table 6). The shades of gray in the dynamical power spectra represent the Leahy power, with darker shades indicating higher powers.

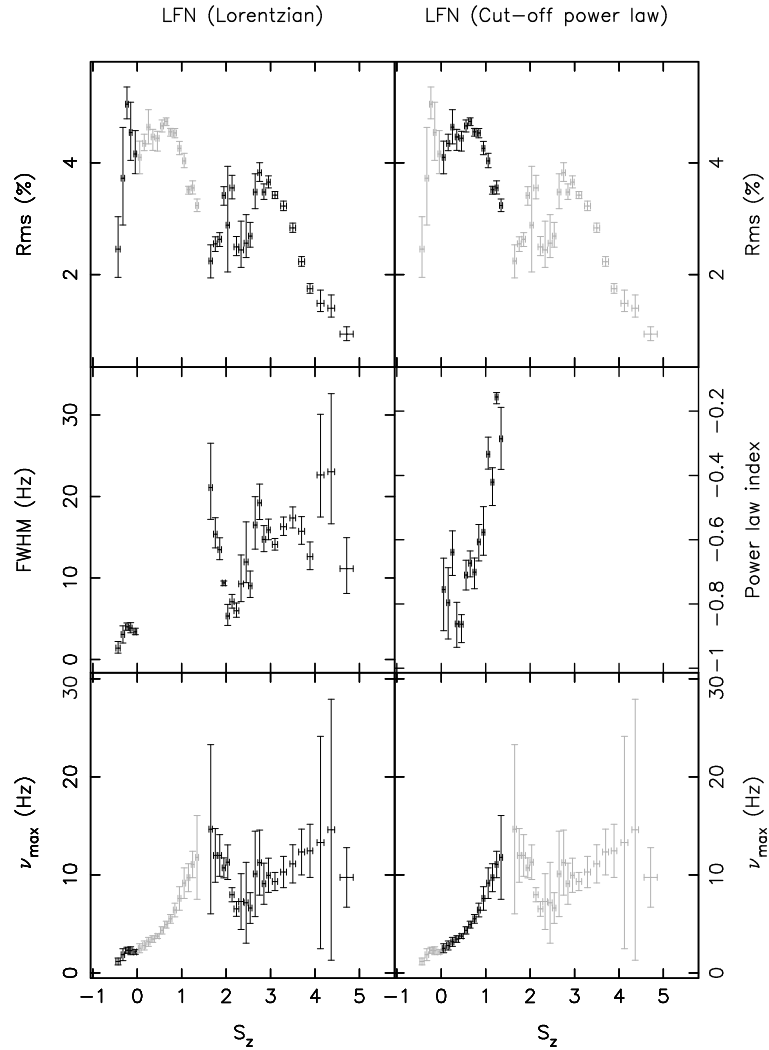


FIG. 10.—LFN properties as function of S_z . The left column shows the results for the fits with a Lorentzian, the right column those for fits with a cut-off power law. In both cases the rms amplitude is the integrated power in the 1–100 Hz range. ν_{max} is the frequency at which most of the power is concentrated (see text for the expressions for ν_{max}). For reasons of comparison we also plotted the values of the other fit function (gray) in the panels for the rms amplitude and ν_{max} .

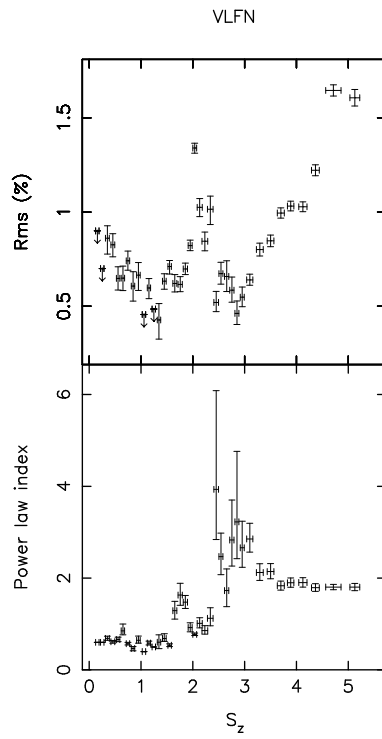


FIG. 11.— VLFN properties as function of S_z . The rms amplitude is the integrated power in the 0.1–1 Hz range. The arrows in the top panel represent upper limits.

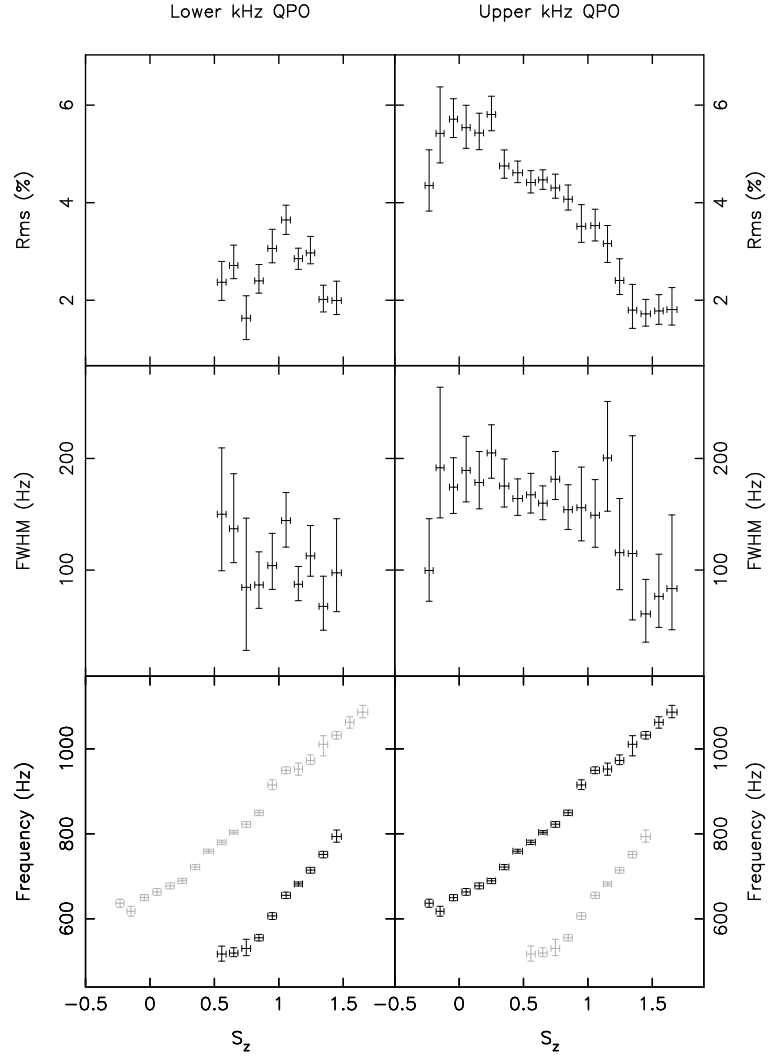


FIG. 12.—kHz QPO properties as a function of S_z . For reasons of comparison, the frequency of the other QPO (gray) is also plotted in the frequency plot of each QPO.

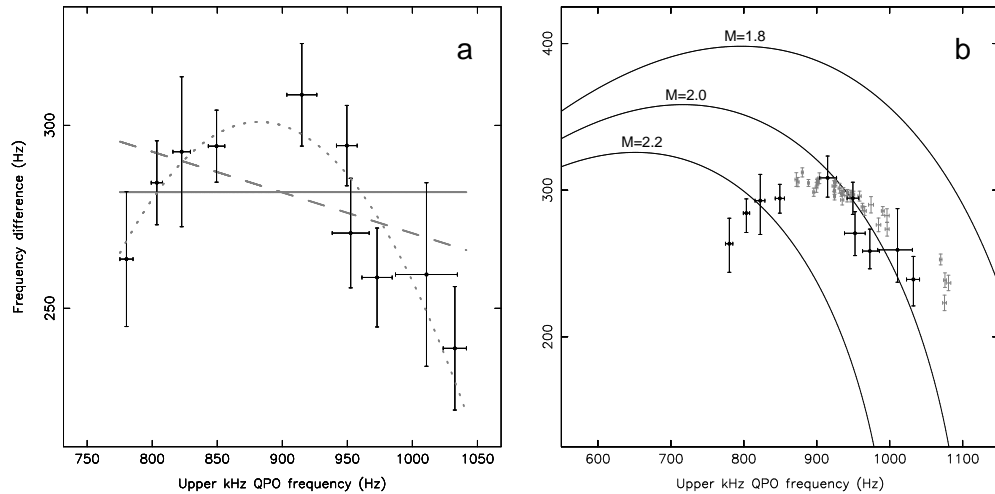


FIG. 13.— The kHz QPO frequency difference in GX 17+2 as function of the upper peak frequency. In (a) three fits to the data are shown (gray): a constant (solid line), a straight line (dashed line), and a parabola (dotted line). In (b) three models for the frequency difference (Stella & Vietri 1999) for three different neutron star masses ($M = 1.8 M_{\odot}$, $M = 2.0 M_{\odot}$, and $M = 2.2 M_{\odot}$) are shown. For comparison we also plotted the data for Sco X-1 (gray) from van der Klis et al. (1997b).

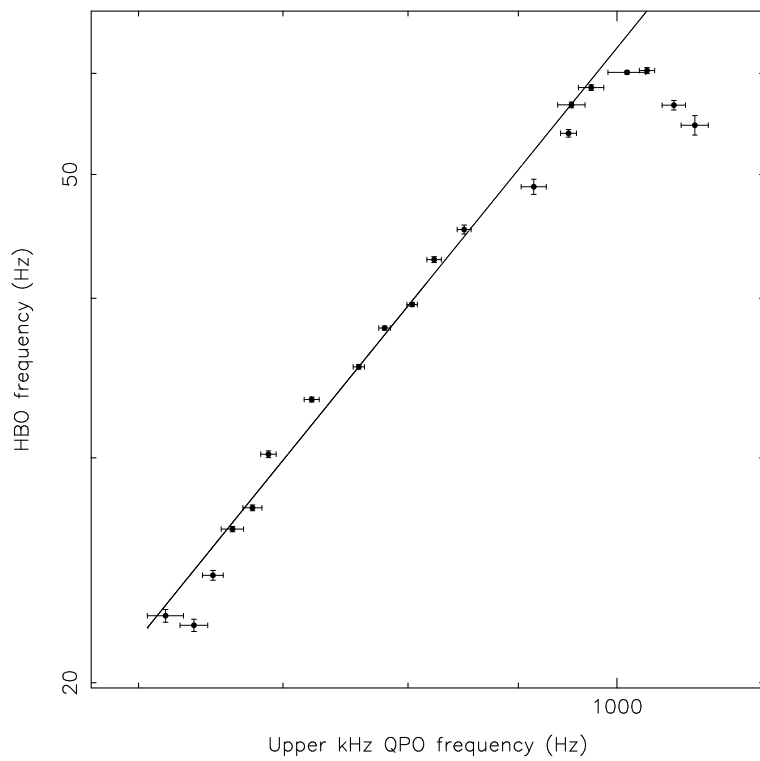


FIG. 14.— HBO frequency as function upper kHz QPO frequency. The solid line is the best power law fit to the data below 1000 Hz for the upper kHz frequency. The power law index is 2.08 ± 0.07 . A clear deviation from this relation can be seen for values above 1000 Hz.

Begin Time (UTC)	End Time (UTC)	Total (ks)	Modes ^a	Gain Epoch
1997-02-02 19:13	1997-02-27 03:34	58.7	3 or 4,5,6,9	3
1997-04-01 19:13	1997-04-04 23:26	34.6	4,5,6,9	3
1997-07-27 02:13	1997-07-28 00:33	42.9	4,5,6,9	3
1998-08-07 06:40	1998-08-08 23:40	71.0	4,5,8	3
1998-11-18 06:42	1998-11-20 13:31	86.0	4,5,(7),8	3
1999-10-03 02:43	1999-10-12 07:05	297.6	10,11,12	4
2000-03-31 12:15	2000-03-31 16:31	6.9	10,11,12	4

^a Modes in addition to the Standard 1 and Standard 2 modes. See Table 2 for modes.

TABLE 1

A LOG OF ALL *RXTE/PCA* OBSERVATIONS USED IN THIS PAPER. MODE 7 WAS NOT ALWAYS ACTIVE DURING THE NOVEMBER 1998 OBSERVATIONS. NOTE THAT NONE OF THE OBSERVATIONS REPRESENTS AN UNINTERRUPTED INTERVAL. EACH IS A COLLECTION OF OBSERVATIONS THAT WERE DONE AROUND THE SAME TIME. THESE OBSERVATIONS WERE SEPARATED IN TIME FROM EACH OTHER FOR VARIOUS REASONS, SUCH AS EARTH OCCULTATIONS, PASSAGES OF THE SOUTH ATLANTIC ANOMALY, OR OBSERVATIONS OF OTHER SOURCES.

Mode	Name	Time Resolution (s)	Energy range (keV)	Energy channels
1	Standard 1	2^{-3}	2–60	1
2	Standard 2	2^4	2–60	129
3	E_8us_8A_0_1s	2^{-17}	2–60	8
4	SB_125us_0_13_1s	2^{-13}	2–5.1	1
5	SB_125us_14_17_1s	2^{-13}	5.1–6.6	1
6	SB_125us_18_23_1s	2^{-13}	6.6–8.7	1
7	SB_125us_18_249_1s	2^{-13}	6.6–60	1
8	E_16us_64M_18_1s	2^{-16}	6.6–60	64
9	SB_125us_24_249_1s	2^{-13}	8.7–60	1
10	SB_125us_0_13_1s	2^{-13}	2–5.8	1
11	SB_125us_14_17_1s	2^{-13}	5.8–7.5	1
12	E_16us_64M_18_1s	2^{-16}	7.5–60	64

TABLE 2

NAMES AND SETTINGS OF THE DATA MODES THAT WERE USED IN OUR ANALYSIS. THE LOWER AND UPPER ENERGY BOUNDARIES OF THE PCA ENERGY SENSITIVITY RANGE ARE GIVEN AS 2 AND 60 KEV, ALTHOUGH THEY CHANGED BETWEEN (AND ALSO SLIGHTLY DURING) THE DIFFERENT GAIN EPOCHS.

Gain Epoch	Soft Color		Hard Color		Intensity	
	(Channels)	(keV)	(Channels)	(keV)	(Channels)	(keV)
3	10–16/5–9	4.8–7.3/3.0–4.8	26–50/17–25	10.5–19.7/7.3–10.5	5–50	3.0–19.7
4	8–13/4–7	4.6–7.1/2.9–4.6	22–42/14–21	10.5–19.6/7.1–10.5	4–42	2.9–19.6

TABLE 3

CHANNEL AND ENERGY BOUNDARIES OF THE SOFT AND HARD COLORS AND THE INTENSITY USED FOR THE SPECTRAL ANALYSIS. THE CHANNEL NUMBERS REFER TO THE STANDARD TWO MODE CHANNELS (1–129).

Component	S_z -range
LFN	-0.6–5.0
HBO (fund.)	-0.6–2.1
HBO (2nd harm.)	-0.6–1.0
HBO (sub-harm.)	-0.6–1.3
Upper kHz QPO	-0.3–1.7
VLFN	0.3–5.5
Lower kHz QPO	0.5–1.5
NBO	1.6–2.1
FBO	2.0–2.7

TABLE 4

THE NINE DIFFERENT COMPONENTS IN THE COMBINED EPOCH 3/EPOCH 4 POWER SPECTRA, AND THE S_z -RANGES IN WHICH THEY WERE DETECTED. THE COMPONENTS ARE LISTED IN ORDER OF S_z APPEARANCE.

S_c	HBO Fundamental			HBO 2 nd Harmonic			HBO Sub-harmonic			NBO		
	Rms ^a (%)	FWHM (Hz)	Frequency (Hz)	Rms ^a (%)	FWHM (Hz)	Frequency (Hz)	Rms ^b (%)	FWHM (Hz)	Frequency (Hz)	Rms ^b (%)	FWHM (Hz)	Frequency (Hz)
-0.43±0.05	4.3±0.7	6 ₋₂ ⁺⁴	21.3±0.8	4.5±0.7	9 ₋₃ ⁺²	41.4±1.4	6.4±1.0	27 ₋₁₀ ⁺¹⁵	0 (fixed)
-0.32±0.04	3.9±0.6	6.9 ₋₁ ^{+2.8}	21.4±0.4	4.9±0.3	11.7±1.7	41.4±0.5	6.9±0.4	19±6	0 (fixed)
-0.23±0.03	2.9±0.3	4.1±0.9	22.2±0.2	3.9±0.2	7.8±1.1	43.9±0.3	7.4±0.3	44±6	0 (fixed)
-0.15±0.03	3.8±0.3	7.3±1.0	22.6±0.3	5.14 _{-0.30} ^{+0.19}	15.8±1.4	43.9±0.4	6.7±0.2	24 ₋₅ ⁺⁸	0 (fixed)
-0.04±0.03	4.02±0.20	8.7±0.9	24.3±0.2	4.79±0.12	15.0±1.0	47.3±0.3	6.41±0.17	19 ₋₄ ⁺⁴	0 (fixed)
0.05±0.03	3.12±0.14	5.4±0.5	26.39±0.13	4.06±0.14	12.7±0.9	50.7±0.2	7.0±0.9	29 ₋₃ ⁺³	0±4
0.16±0.03	3.21±0.18	6.1±0.6	27.42±0.14	3.82±0.13	12.4±0.9	53.7±0.3	6.6 _{-0.9} ^{+1.7}	31±4	2 ₋₃ ⁺³
0.25±0.03	3.54±0.17	8.8±0.7	30.20±0.18	3.73±0.12	16.4±1.2	57.9±0.4	5.7±0.8	25±3	8 ₋₃ ⁺⁶
0.35±0.04	2.81±0.11	6.8±0.5	33.33±0.15	2.86±0.12	15.0±1.3	63.6±0.4	5.2 _{-0.9} ^{+1.7}	32 ₋₃ ⁺⁵	9 ₋₈ ⁺²
0.46±0.04	2.95±0.11	8.3±0.5	35.35±0.15	2.61±0.09	13.9±1.2	68.5±0.4	4.6 _{-0.9} ^{+0.4}	28±3	10 ₋₈ ^{+1.8}
0.56±0.03	2.75±0.09	8.3±0.5	37.91±0.14	2.41±0.08	13.6±1.1	73.4±0.3	4.1±0.4	26±3	15.0±1.5
0.65±0.03	2.57±0.10	7.8±0.6	39.56±0.14	2.42±0.09	16.8±1.5	77.9±0.5	3.9±0.2	28±3	18.0±1.0
0.75±0.03	2.41±0.13	9.1±0.9	42.9±0.2	1.92±0.11	14.5±1.9	83.3±0.7	3.6±0.3	28±4	20.6±1.0
0.85±0.03	2.2±0.2	9.8±1.6	45.3±0.4	1.62±0.15	13±3	89.4±0.9	3.2±0.3	29±5	24.9±1.4
0.95±0.03	2.3±0.3	13.3±	48.9±0.7	1.8±0.2	22 ₋₅ ⁺⁸	93±2	2.5±0.4	21±7	25.2±1.3
1.06±0.03	1.52±0.17	6.0±1.3	53.9±0.4	1.09±0.15	15 (fixed)	107 (fixed)	2.76 _{-0.19} ^{+0.26}	31±7	32.2±1.6
1.15±0.03	1.40±0.12	5.1±1.0	56.7±0.3	<0.7	15 (fixed)	113 (fixed)	2.5 _{-0.2} ^{+0.2}	32±6	35.5±1.6
1.25±0.03	1.42±0.12	5.1 _{-0.3} ^{+0.6}	58.5±0.3	2.8 _{-0.3} ^{+0.3}	57 ₋₁₂ ⁺¹⁷	41±6
1.35±0.03	1.63±0.11	4.0±0.6	60.11±0.17	< 2.5	21±14	43±3
1.45±0.04	1.40±0.12	5.2±1.2	60.3±0.3
1.55±0.03	1.8±0.2	14±3	56.7 _{-0.5} ^{+0.8}
1.65±0.04	1.72±0.14	12±3	54.6±1.0	1.7±0.2	3.8±0.7	6.33±0.16	
1.76±0.04	1.99±0.12	17±3	53.6±1.0	2.07±0.11	2.08±0.20	6.82±0.04	
1.86±0.04	1.90±0.12	17±3	52.6±1.1	2.89±0.08	2.13±0.11	6.91±0.03	
1.95±0.04	1.80±0.16	19±4	50.1±1.2	2.94±0.12	2.11±0.13	6.96±0.02	
2.04±0.04	1.2±0.2	11 ₋₅ ⁺⁷	48.2±2	3.2±0.2	3.7±0.4	6.86±0.10	
2.13±0.05	<1.2	9 (fixed)	46 (fixed)	2.8±0.8	5.4 ₋₁ ^{+0.6}	13.9 _{-0.4} ^{+0.6}	
2.23±0.06	4.93±0.11	5.1±0.2	14.78±0.08	
2.34±0.05	5.60±0.07	6.4±0.18	15.44±0.06	
2.45±0.05	5.28±0.11	8.1±0.3	16.75±0.12	
2.54±0.04	4.37±0.17	10.3±0.7	18.2±0.2	
2.65±0.04	3.36±0.20	13.6±1.6	19.7±0.6	
2.75±0.04	1.8±0.4	8±4	23.1±0.9	
							< 1.8	10 (fixed)	25 (fixed)	

^a Integrated between $-\infty$ Hz and $+\infty$ Hz.

^b Integrated between 0 Hz and $+\infty$ Hz, because of low Q values.

TABLE 5
FIT RESULTS FOR THE LOW FREQUENCY QPOS.

Interval	Count Rate (counts s ⁻¹)	Fractional rms (%)	Absolute rms (counts s ⁻¹)
Nov 1998 - I	2811	2.58±0.19	72.5±5.3
Nov 1998 - II	2648	3.2±0.3	85±8
Nov 1998 - III	4568	<0.71	<32.4
Nov 1998 - IV	3232	<2.1	<68
Nov 1998 - V	2833	3.3±0.2	93±6
Oct 1999 - I	1742	5.56±.17	96.9±3.0
Oct 1999 - II	2616	<1.57	<41.1
Oct 1999 - III	1847	4.3±0.4	79±7

TABLE 6

THE PROPERTIES OF THE NBO/FBO DURING THE TWO BURSTS SHOWN IN FIGURE 9. THE INTERVALS GIVEN IN FIRST COLUMN CAN BE ALSO FOUND IN THAT FIGURE. THE UPPER LIMITS IN THE LAST TWO COLUMNS ARE 95% CONFIDENCE. THE COUNT RATES ARE IN THE 5.1–60 KEV (NOVEMBER 1998, 5 PCUS) AND 5.8–60 KEV (OCTOBER 1999, 3 PCUS) BANDS.

S_z	VLFN		LPN (Cut-off power law)			LPN (Lorentzian)		
	Rms ^a (%)	Index	Rms ^b (%)	Index	Cut-off (Hz)	Rms ^b (%)	FWHM (Hz)	Frequency (Hz)
-0.43±0.05	2.5±0.5	1.4±0.7	0.9±0.3
-0.32±0.04	3.7±0.9	3.1±1.0	1.05±0.19
-0.23±0.03	5.0±0.3	4.0±0.4	1.15±0.13
-40.15±0.03	4.5±0.5	3.9±0.6	1.19±0.09
-0.04±0.03	4.2±0.4	3.4±0.4	1.30±0.06
0.05±0.03	4.1±0.3	-0.76±0.11	1.43±0.15
0.16±0.03	<0.9	0.6 (fixed)	4.35±0.15	-0.80±0.11	1.56 ^{+0.16} _{-0.16}
0.25±0.03	<0.7	0.6 (fixed)	4.6±0.3	-0.64±0.07	1.93±0.19
0.35±0.04	0.86±0.07	0.69±0.04	4.46 ^{+0.14} _{-0.24}	-0.86±0.07	1.85 ^{+0.12} _{-0.08}
0.46±0.04	0.83±0.06	0.61±0.03	4.44 ^{+0.13} _{-0.23}	-0.86 ^{+0.03} _{-0.06}	2.01 ^{+0.06} _{-0.12}
0.56±0.03	0.65±0.06	0.66±0.05	4.66±0.11	-0.71±0.05	2.54±0.14
0.65±0.03	0.65±0.06	0.85 ^{+0.15} _{-0.09}	4.74±0.07	-0.67±0.04	2.94±0.12
0.75±0.03	0.74±0.05	0.57±0.03	4.55±0.07	-0.70±0.05	3.24±0.14
0.85±0.03	0.61±0.08	0.47±0.05	4.53±0.08	-0.61±0.06	4.0±0.2
0.95±0.03	0.67±0.07	0.64 ^{+0.09} _{-0.06}	4.26±0.12	-0.58±0.08	4.8±0.4
1.06±0.03	<0.5	0.4 (fixed)	4.04±0.13	-0.33±0.05	6.9±0.6
1.15±0.03	0.60±0.05	0.58±0.04	3.52±0.07	-0.42 ^{+0.04} _{-0.07}	6.8±0.4
1.25±0.03	<0.5	0.5 (fixed)	3.55±0.12	-0.156 ^{+0.04} _{-0.021}	9.6 ^{+0.4} _{-0.8}
1.35±0.03	0.43±0.09	0.60±0.15	3.24±0.11	-0.29±0.10	9.2±1.2
1.45±0.04	0.63±0.04	0.68 ^{+0.10} _{-0.06}
1.55±0.03	0.71±0.04	0.54±0.03
1.65±0.04	0.62±0.05	1.29±0.19	2.2±0.3	21±5	10±2
1.76±0.04	0.62±0.04	1.6 ±0.2	2.55±0.13	15.4±1.8	9.2±0.7
1.86±0.04	0.70±0.03	1.48±0.14	2.63±0.12	13.5±1.3	9.9±0.6
1.95±0.04	0.82±0.03	0.92±0.10	3.42±0.17	9.4±0.3	9.6±0.3
2.04±0.04	1.34±0.03	0.77±0.03	2.9±0.9	5.3±1.3	11.0±0.5
2.13±0.05	1.03±0.05	1.01±0.11	3.6±0.2	7.1±0.8	7.1±0.20
2.23±0.06	0.85±0.05	0.86 ^{+0.11} _{-0.07}	2.50±0.17	6.0±0.9	5.8±0.2
2.34±0.05	1.02±0.08	1.12 ^{+0.23} _{-0.16}	2.4 ^{+0.5} _{-0.3}	9 ⁺⁴ ₋₂	5.6±0.7
2.45±0.05	0.52±0.05	3.93 ^{+2.2} _{-1.1}	2.6 ^{+0.3} _{-0.3}	12 ⁺⁵ ₋₃	3.9 ^{+0.7} _{-0.4}
2.54±0.04	0.67±0.06	2.5±0.4	2.7 ^{+0.2} _{-0.2}	9.0±1.6	4.8 ^{+1.0} _{-0.4}
2.65±0.04	0.66±0.08	1.7±0.4	3.5±0.3	16±3	5.8±0.7
2.75±0.04	0.59±0.07	2.8 ^{+0.9} _{-0.6}	3.82±0.17	19±3	5.9±0.4
2.85±0.04	0.46±0.06	3.2 ^{+1.8} _{-0.8}	3.48±0.14	14.7±1.6	5.3±0.4
2.95±0.04	0.55±0.05	2.7±0.5	3.66±0.11	15.9±1.3	6.0±0.4
3.10±0.06	0.64±0.03	2.6±0.3	3.42±0.06	14.1±0.7	6.1±0.2
3.29±0.07	0.80±0.03	2.12±0.18	3.23±0.09	16.3±1.1	6.3 ±0.4
3.50±0.07	0.85±0.03	2.14±0.16	2.84±0.08	17.4±1.3	7.0±0.5
3.70±0.07	1.00±0.03	1.83±0.10	2.23±0.09	15.7±1.7	9.5±0.5
3.89±0.06	1.03±0.03	1.90±0.10	1.75±0.09	12.6±1.7	10.7±0.7
4.12±0.08	1.03±0.03	1.90±0.10	1.49 ^{+0.24} _{-0.15}	23 ⁺⁷ ₋₅	7.0 ^{+2.0} _{-3.5}
4.37±0.08	1.22±0.03	1.79±0.08	1.40 ^{+0.24} _{-0.16}	23 ⁺¹⁰ ₋₇	9 ⁺² ₋₃
4.71±0.15	1.65±0.03	1.81±0.06	0.94±0.12	11 ⁻³	8 (fixed)
5.13±0.10	1.61±0.04	1.80±0.08	< 0.6	11 (fixed)	8 (fixed)

^a Integrated between 0.1 Hz and 1 Hz

^b Integrated between 1 Hz and 100 Hz

TABLE 7
FIT RESULTS FOR THE NOISE COMPONENTS AT LOW FREQUENCIES.

S_z	Lower kHz QPO			Upper kHz QPO			Difference (Hz)
	Rms (%)	FWHM (Hz)	Frequency (Hz)	Rms (%)	FWHM (Hz)	Frequency (Hz)	
-0.32±0.04	<7	140 ⁺¹³⁴ ₋₆₈	641 ⁺³⁵ ₋₂₀	...
-0.23±0.03	4.4±0.6	100 ⁺⁴⁶ ₋₂₈	637±9	...
-0.15±0.03	5.4 ^{+1.0} _{-0.6}	192 ⁺²⁷ ₋₄₅	618±12	...
-0.04±0.03	5.7±0.4	174 ⁺²⁵ ₋₂₅	650±7	...
0.05±0.03	5.5±0.4	189±29	663±8	...
0.16±0.03	5.4±0.4	178±26	678±7	...
0.25±0.03	5.8±0.4	205±24	689±6	...
0.35±0.04	4.8±0.3	175±21	722±6	...
0.46±0.04	<2.0	130 (<i>fixed</i>)	475 (<i>fixed</i>)	4.6±0.2	164±16	759±5	...
0.56±0.03	2.4±0.4	145±55	517±18	4.4±0.2	167±18	780±18	263±18
0.65±0.03	2.7 ^{+0.4} _{-0.3}	137 ⁺⁴⁹ ₋₃₀	519 ⁺¹³ ₋₉	4.46±0.20	160±15	804±4	284±11
0.75±0.03	1.6±0.4	85±59	530±20	4.3±0.2	181±21	823±7	293±20
0.85±0.03	2.4±0.3	87±25	555±8	4.0±0.3	154±20	849±6	294±10
0.95±0.03	3.1±0.3	104±25	607±8	3.5±0.4	156±33	915±11	308±14
1.06±0.03	3.6±0.3	144±24	655±8	3.5±0.3	149±30	950±8	294±11
1.15±0.03	2.9±0.2	87±15	682±5	3.2±0.4	200±49	953±14	271±15
1.25±0.03	3.0 ^{+0.3} _{-0.2}	112 ⁺²⁷ ₋₈	714±7	2.4 ^{+0.4} _{-0.3}	116 ⁺⁴⁹ ₋₃₃	973±11	258±13
1.35±0.03	2.0±0.3	67±24	752±8	1.8±0.4	115 ⁺¹⁰⁶ ₋₆₀	1011±24	259±25
1.45±0.04	2.0±0.3	98±41	794±14	1.7±0.3	61±28	1033±9	239±17
1.55±0.03	<2.3	80±59	830±19	1.8±0.3	76±32	1063±13	...
1.65±0.04	1.8 ^{+0.5} _{-0.3}	83 ⁺⁶⁶ ₋₃₇	1087±15	...
1.76±0.04	<1.5	90 (<i>fixed</i>)	1085 (<i>fixed</i>)	...

TABLE 8
FIT RESULTS FOR THE HIGH FREQUENCY QPOS.